Beyond Battery State of Charge Estimation: Observer for Electrode-Level State and Cyclable Lithium With Electrolyte Dynamics

Dong Zhang[®], Saehong Park[®], Luis D. Couto[®], Venkatasubramanian Viswanathan[®], and Scott J. Moura[®], *Member, IEEE*

Abstract—This article presents a provably convergent battery estimation scheme based on a single particle model with electrolyte (SPMe) dynamics, by proposing a systematic methodology to estimate critical information such as electrodelevel states, electrolyte dynamics, and cyclable lithium. Electrode-level state estimation suffers from weak observability originating from two standalone electrode dynamics, which is then aggravated by the addition of electrolyte dynamics. This lack of observability can be alleviated by exploiting lithium inventory conservation enabled by the Kalman decomposition, allowing one to separate out the unobservable subspace. Assuming the knowledge of cyclable lithium, a nonlinear state observer with provable convergence can be constructed for the SPMe model, using voltage and current measurements. To relax this strong assumption, a sensitivity-based parameter estimation scheme is also deployed to track cyclable lithium—a crucial physical variable for capacity fade. Ultimately, the estimation framework can perform finer monitoring and diagnosis of battery charge and health down to the level of individual electrode and the electrolyte. Experimental validation demonstrates <1% estimation error for cyclable lithium inventory. Solid phase lithium concentration estimates, especially in the negative electrode, can be sensitive to disturbances in cyclable lithium.

Index Terms—Kalman decomposition, lithium-ion (Li-ion) batteries, nonlinear state observer, parameter estimation.

I. INTRODUCTION

ITHIUM-ION (Li-ion) batteries form a crucial piece of wide dissemination of electric vehicles and renewable energy resources, propelled by the high efficiency and high energy and power densities [1]. However, batteries must be carefully monitored to ensure sufficient life and manage abuse conditions such as over-(dis)charge; otherwise, they might exhibit accelerated aging in the best cases and become a safety hazard in the most extreme cases. Battery monitoring

Manuscript received 17 February 2022; revised 1 June 2022; accepted 7 July 2022. Date of publication 14 July 2022; date of current version 21 December 2023. (Corresponding author: Venkatasubramanian Viswanathan.)

Dong Zhang is with the School of Aerospace and Mechanical Engineering, The University of Oklahoma, Norman, OK 73019 USA (e-mail: dzhang@ou.edu).

Saehong Park and Scott J. Moura are with the Department of Civil and Environmental Engineering, University of California at Berkeley, Berkeley, CA 94720 USA (e-mail: sspark@berkeley.edu; smoura@berkeley.edu).

Luis D. Couto is with the Department of Control Engineering and System Analysis, Université Libre de Bruxelles, 1050 Brussels, Belgium (e-mail: lcoutome@ulb.ac.be).

Venkatasubramanian Viswanathan is with the Department of Mechanical Engineering, Carnegie Mellon University, Pittsburgh, PA 15213 USA (e-mail: venkvis@cmu.edu).

Digital Object Identifier 10.1109/TTE.2022.3191136

involves the estimation of meaningful physical states, with state of charge (SOC) and state of health (SOH) as two most crucial figures of merit [2]. While SOC is the battery energy fuel gauge, typical SOH indicators include battery capacity and internal resistance. These different battery states need to be inferred from data since they cannot be directly measured during regular operation. The state estimation problem in batteries is challenging because: 1) internal states exhibit weak observability under traditional voltage and current sensing; 2) output measurements and internal states have notoriously nonlinear relationships; and 3) electrochemical processes evolve significantly with temperature and time. Solutions to these problems offer a huge opportunity for advanced control of battery systems. This is especially true if the resulting estimation algorithms at the core of battery management systems (BMSs) are able to determine electrochemical quantities beyond classical SOC and SOH, e.g., electrolyte concentration or lithium inventory.

The battery state estimation problem has been thoroughly investigated in the literature [3]-[7]. These methods may be divided into three categories depending on their underlying mathematical models, namely, data-driven models, gray-box models, and electrochemical models. The models belonging to the data-driven category are very flexible and provide accurate approximations. However, they lack physical interpretation and require excessive data for training [8]. The second category involves model abstractions of battery processes, such as the electric circuit analogy used in equivalent circuit models (ECMs) for battery representation. Although these models can be accurate if properly tuned, they do not explicitly represent relevant electrochemical processes governing battery dynamics [9]. In the last category, electrochemical models are capable of capturing the physical phenomena inside a Li-ion battery, such as transport, reaction kinetics, mass, and charge conservation. Therefore, electrochemical models are among the best candidates for characterizing the present operational status of a battery, in which the Doyle-Fuller-Newman (DFN) model [10] has become the benchmark par excellence. However, its computational burden hinders its applicability for real-time estimation/control despite recent advancement on adopting circuit theory to draw analogy with electrochemical models [11], [12]. Thus, reduced-order electrochemical models become extremely useful, e.g., the widely popular single particle model (SPM) family [13]. The SPM is recognized

2332-7782 © 2022 IEEE. Personal use is permitted, but republication/redistribution requires IEEE permission. See https://www.ieee.org/publications/rights/index.html for more information.

as striking a good balance between model complexity and accuracy at relatively low current densities [14]. Enhanced versions of the SPM have been derived to extend its application range, such as the inclusion of electrolyte [15]–[19] or aging dynamics [15], [16], [20]–[22].

A well-known model simplification for an electrochemical model is to deal with one of the electrodes and ignore the other. This modeling choice is motivated by the weak system observability when lithium concentration in both electrodes to be estimated simultaneously [23]–[25]. Negative electrodes, typically graphite, are often kept since they are more prone to degradation and have slower diffusion times compared to positive electrodes [26]. Positive electrodes have also been retained for observer design, on the basis that larger opencircuit potential (OCP) slopes improve observability [18]. The single-electrode approximation can be obtained by assuming either: 1) the neglected electrode is modeled in open loop or 2) total moles of lithium are preserved. In case 1), one electrode provides a pseudo voltage measurement via open-loop simulation, while the state of the other electrode is estimated in a closed-loop manner, giving rise to Kalman filters (KFs) and particle filters [27]. Although relatively simple to implement, this option produces biased state estimates when the open-loop electrode model is wrongly initialized. In case 2), conservation of lithium adds an algebraic constraint that is used for observer design. This option is the most explored one through KFs [24], sliding mode observers [28], and nonlinear observers [29], by taking advantage of the assumption that the states of two electrodes are linearly dependent on each other. Therefore, case 2) properly initializes the state estimators given knowledge of total solid phase lithium inventory to ensure accurate electrode state estimation.

More recent contributions avoid the aforementioned single-electrode simplification and instead pursue state estimation of both electrodes simultaneously, denoted as electrodelevel estimation. This new estimation paradigm offers the possibility of differentiating the state of each electrode individually, which opens the door to finer monitoring of degradation mechanisms at the electrode level [30]. Three approaches exist to alleviate the observability issues arising from the electrode-level estimation. The first one focuses on improving observability by exploiting extra measurements, such as temperature [31], besides classical current and voltage, at the expense of additional instrumentation, added cost, and data processing requirements. The second approach consists of an interconnected type of observer, where each electrode state is estimated separately by a dedicated observer, but the two observers exchange information, which contributes to the convergence of the estimation scheme [32], [33]. However, the structure of interconnected observers might be complex. A third approach relies on partial differential equation (PDE) models to design either Luenberger [34] or backstepping [18] observers, which again require lithium mass conservation for observer gain design. Even if these contributions propose relevant approaches for electrode-level estimation, these methodologies lack rigorous observability analysis, neglect crucial battery dynamics, e.g., electrolyte, and often assume prior knowledge of a time-invariant lithium inventory.

Apart from electrode-level estimation, there are other electrochemical quantities of interest that influence battery performance. One of them is electrolyte dynamics, which need to be coupled with the SPM for a more comprehensive representation of a battery subject to large current rates. The electrolyte state estimation problem, however, has received little attention from the research community. Contributions to this topic include a moving horizon estimator [35], a particle filter [36], and an extended Kalman filter (EKF) [37], all proposed based on the DFN model, as well as a Luenberger observer [17], an open-loop observer [18], and an unscented KF [38] using reduced-order electrochemical models. Another important quantity is the cyclable moles of lithium, which is regarded as one of the primary indicators for battery degradation. The estimation of this quantity can be related to the loss of lithium inventory that may be experimentally determined from open-circuit voltage (OCV) measurements [39] or via electrochemical techniques such as incremental capacity [40] or differential voltage analyses [41]. Lithium inventory can also be seen as a model parameter in electrochemical models and its estimation can be formulated as a parameter identification problem. In this context, several parameter estimation techniques have been used, including a nonlinear least-squares method [26], EKFs [42], [43], and a Levenberg-Marquardt (L-M) method [44]. As we will demonstrate later, knowledge of lithium inventory would enable decomposition of the SPMe model and the mathematically guaranteed state observer convergence.

Observability analysis in battery electrochemical modelbased SOC/SOH estimation has been overlooked. Among the studies that explored electrochemical model observability, most have been focusing on SPM without electrolyte dynamics [31], [45], [46]. It was only in recent years that observability analysis for single particle model with electrolyte (SPMe) dynamics is attracting attention [27], [47], [48]. In this study, we perform a comprehensive analysis on the observability of the states in the SPMe in a mathematically elegant way using the Kalman decomposition. The SPMe model describes the dynamic behaviors in two electrodes (solid phase) as well as in the electrolyte (electrolyte phase). The adopted Kalman decomposition technique brings a system to a structure where the observable and unobservable components are clearly separated. Then, the lithium concentration in the solid phase of the two electrodes as well as in the electrolyte phase can be estimated from current and voltage measurements via a nonlinear state observer based on the transformed system. As will be demonstrated later, the analysis presented here explores the conservation of moles of lithium, so we will propose a sensitivity-based parameter identification scheme adopting the L-M algorithm, which outputs estimates for total moles of lithium. The proposed framework is a significant improvement over the preliminary work in [49], which only addressed the electrode-level estimation problem for an SPM without considering battery aging and electrolyte dynamics. In particular, the main contributions of this work include the following:

- 1) a state observability analysis on the SPMe dynamics;
- a rigorous parameter estimation scheme to recursively update lithium inventory while battery aging,

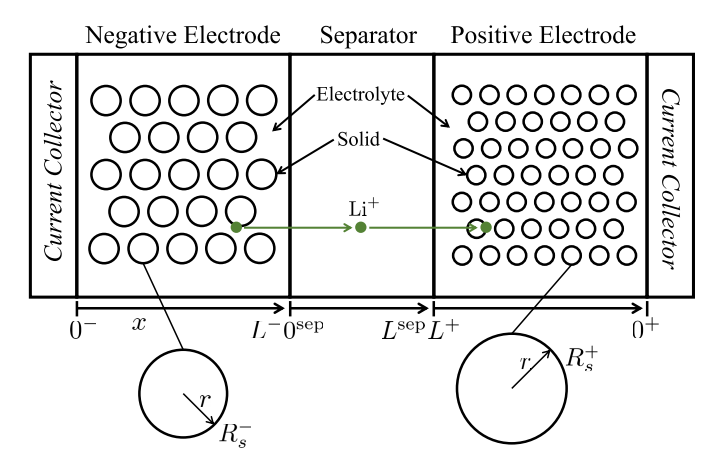


Fig. 1. Sketch of a Li-ion battery cross-sectional geometry.

thus enhancing the state estimation algorithm applicability.

The estimation framework will monitor solid phase lithium concentration, electrolyte phase lithium concentration, and solid phase lithium inventory in a mathematically guaranteed fashion and can be interpreted as an online strategy for electrochemical model-based simultaneous SOC (critical lithium concentration) and SOH (lithium inventory) estimation.

II. MODEL DEVELOPMENT

In this section, we discuss common assumptions for deriving an SPMe dynamics from a DFN model. We introduce the electrochemical principles of the batteries very briefly, and readers may refer to [1], [10], and [52] for a more comprehensive discussion. Fig. 1 showcases a schematic summary of the DFN model, demonstrating the solid phase and electrolyte phase spreading across three domains of the cell: anode (negative electrode), separator, and cathode (positive electrode). This model is capable of predicting the spatial and temporal evolution of lithium concentrations ($c_s^{\pm}(x, r, t)$) and $c_e(x,t)$), electric potentials $(\phi_s(x,t))$ and $\phi_e(x,t)$), ionic current $i_e(x,t)$, and molar ion fluxes $j_n^{\pm}(x,t)$. A complete definition of model parameters and state variables is given in Table I. In order to simplify the formidable complexity of the DFN model, the literature has presented a rich set of strategies for model reduction. One of the notable ones resorts to the SPMe [18], [51]–[53], which seeks to preserve modeling fidelity, particularly at high current rates. The key assumption that enables the derivation of SPMe is that the solid phase lithium concentration, exchange current density, and molar ion flux are constant along the spatial coordinate x. Subsequently, SPMe model equations and model analysis will be provided.

A. Governing Equations and Boundary Conditions

This section presents the set of mathematical equations for SPMe. The main components of the model are inherited from [18], with modifications for the purpose of state observability analysis and a provably convergent observer design.

The solid phase lithium diffusion phenomenon can be characterized by Fick's laws of diffusion over a spherical domain $r \in [0, R_s^{\pm}]$, which characterizes the evolution of lithium

TABLE I SPME MODEL SYMBOL DESCRIPTION

Symbols	Description				
a^{\pm}	Specific interfacial surface area				
A	Cell cross sectional area				
c_s^{\pm}	Solid phase lithium concentration				
c_e^j	Electrolyte phase lithium concentration				
c_{ss}^{\pm}	Lithium concentration at particle surface				
\bar{c}_s^{\pm}	Volume-averaged lithium concentration				
$a^- \ A \ c_s^+ \ c_{ss}^- \ c_{ss}^- \ c_{s,\max}^+ \ \phi_s^+ \ \phi_s$	Max lithium concentration in solid phase				
ϕ_s^{\pm}	Solid phase electric potential				
ϕ_e	Electrolyte phase electric potential				
j_n^{\pm}	Molar ion flux				
$\phi_{e}^{s} \ \phi_{e}^{e} \ j_{n}^{\pm} \ i_{e}^{\pm} \ i_{0}^{\pm} \ \eta^{\pm} \ D_{s}^{\pm}, D_{e}$	Ionic current				
i_0^{\pm}	Exchange current density				
$\eta^{\stackrel{\smile}{\pm}}$	Overpotential				
D_s^{\pm}, D_e	Diffusivity in solid, electrolyte phase				
$f_{c/a} \ F$	Molar activity coefficient in electrolyte				
\acute{F}	Faraday's constant				
I	Applied current				
V_{\cdot}	Terminal voltage				
k^{\pm}	Charge transfer reaction rate				
L^j	Electrode thickness				
$n_{ m Li,s}$	Total moles of lithium in solid phase				
$n_{ m Li,e}$	Total moles of lithium in electrolyte phase				
σ^{\pm} , κ	Conductivity in solid, electrolyte phase				
R_{-}	Universal gas constant				
$R_{s}^{\pm} \ R_{s}^{\pm} \ t_{c}^{0} \ T$	Contact film resistance				
R_s^{\pm}	Particle radius				
t_c^0	Transference number				
$T_{_{\perp}}$	Temperature				
U^{\pm}	Open circuit potential				
α^{\pm}	Charge transfer coefficient				
$\varepsilon_s^{\pm}, \varepsilon_e$	Volume fraction of solid, electrolyte phase				

concentration within a spherical electrode

$$\frac{\partial c_s^+}{\partial t}(r,t) = D_s^+ \left[\frac{\partial^2 c_s^+}{\partial r^2}(r,t) + \frac{2}{r} \frac{\partial c_s^+}{\partial r}(r,t) \right] \tag{1}$$

$$\frac{\partial c_s^-}{\partial t}(r,t) = D_s^- \left[\frac{\partial^2 c_s^-}{\partial r^2}(r,t) + \frac{2}{r} \frac{\partial c_s^-}{\partial r}(r,t) \right]$$
(2)

with Neumann boundary conditions

$$\frac{\partial c_s^+}{\partial r}(0,t) = 0, \quad D_s^+ \frac{\partial c_s^+}{\partial r}(R_s^+,t) = -j_n^+(t) \tag{3}$$

$$\frac{\partial c_s^-}{\partial r}(0,t) = 0, \quad D_s^- \frac{\partial c_s^-}{\partial r} (R_s^-,t) = -j_n^-(t). \tag{4}$$

The intercalation current density $j_n^{\pm}(t)$ is assumed constant with respect to x along the cell thickness. This assumption makes it possible to represent $j_n^{\pm}(t)$ as

$$j_n^+(t) = -\frac{1}{Fa^+AL^+}I(t), \quad j_n^-(t) = \frac{1}{Fa^-AL^-}I(t)$$
 (5)

which depends on the battery current in a linear fashion. The Butler-Volmer equation depicts the relation between the current density and the overpotentials via

$$j_n^{\pm}(t) = \frac{1}{F} i_0^{\pm}(t) \left[\exp\left(\frac{\alpha F}{RT} \eta^{\pm}\right) - \exp\left(-\frac{(1-\alpha)F}{RT} \eta^{\pm}\right) \right]$$
(6)

where the exchange current density $i_0^{\pm}(t)$ is given by

$$i_0^{\pm}(t) = k^{\pm} \sqrt{c_{e,0}^{\pm}(t)c_{ss}^{\pm}(t)\left(c_{s,\text{max}}^{\pm} - c_{ss}^{\pm}(t)\right)}$$
 (7)

with $c_{ss}^{\pm}(t)=c_s^{\pm}(R_s^{\pm},t)$ and $c_{e,0}^{\pm}$ denotes a nominal value of the electrolyte phase concentration. Specifically, in this work, $c_{e,0}^{+}(t)=c_e^{+}(0^+,t)$ and $c_{e,0}^{-}(t)=c_e^{-}(0^-,t)$ are electrolyte phase concentrations at the battery terminals. This is a crucial property to enable a provable convergent estimator design, which will be highlighted later. The overpotentials in (6), η^{\pm} , can be computed by the difference between the solid and electrolyte potentials minus the equilibrium potentials. Mathematically,

$$\eta^{\pm}(t) = \phi_s^{\pm}(x,t) - \phi_e(x,t) - U^{\pm}(c_{ss}^{\pm}(t)) - FR_f^{\pm}j_n^{\pm}(t).$$
 (8)

The lithium concentration in the electrolyte phase is primarily driven by diffusion of Li-ions and the current

$$\varepsilon_e^+ \frac{\partial c_e^+}{\partial t}(x,t) = D_{e,\text{eff}}^+ \frac{\partial^2 c_e^+}{\partial x^2}(x,t) - \frac{\left(1 - t_c^0\right)}{FAL^+} I(t) \tag{9}$$

$$\varepsilon_e^{\text{sep}} \frac{\partial c_e^{\text{sep}}}{\partial t}(x, t) = D_{e, \text{eff}}^{\text{sep}} \frac{\partial^2 c_e^{\text{sep}}}{\partial x^2}(x, t)$$
 (10)

$$\varepsilon_e^{-} \frac{\partial c_e^{-}}{\partial t}(x,t) = D_{e,\text{eff}}^{-} \frac{\partial^2 c_e^{-}}{\partial x^2}(x,t) + \frac{\left(1 - t_c^0\right)}{FAL^{-}} I(t) \quad (11)$$

where $D_{e,\mathrm{eff}}^j=D_e^j\cdot(\varepsilon_e^j)^{\mathrm{brug}}$, with $j\in\{+,-,\mathrm{sep}\}$. Furthermore, the concentration and ion flux must be continuous at the domain boundaries

$$\frac{\partial c_e^-}{\partial x}(0^-, t) = \frac{\partial c_e^+}{\partial x}(0^+, t) = 0 \tag{12}$$

$$c_{\ell}^{-}(L^{-},t) = c_{\ell}^{\text{sep}}(0^{\text{sep}},t)$$
 (13)

$$c_e^{\text{sep}}(L^{\text{sep}}, t) = c_e^+(L^+, t) \tag{14}$$

$$\varepsilon_e^- D_e^- \frac{\partial c_e^-}{\partial x} (L^-, t) = \varepsilon_e^{\text{sep}} D_e^{\text{sep}} \frac{\partial c_e^{\text{sep}}}{\partial x} (0^{\text{sep}}, t)$$
 (15)

$$\varepsilon_e^{\text{sep}} D_e^{\text{sep}} \frac{\partial c_e^{\text{sep}}}{\partial x} (L^{\text{sep}}, t) = \varepsilon_e^+ D_e^+ \frac{\partial c_e^+}{\partial x} (L^+, t). \tag{16}$$

The diffusion dynamics (1) and (2) and (9)–(11) may be further enhanced by accounting for concentration-dependent diffusion coefficients [54], [55]. This work neglects this feature to seek the balance between model accuracy and simplicity. Not including the concentration-dependent diffusion coefficients introduces modeling uncertainty, but we expect the proposed state observer in Section V to be robust.

The potentials in solid phase and electrolyte phase are governed by

$$\frac{\partial \phi_s^{\pm}}{\partial x}(x,t) = \frac{i_e^{\pm} - I(t)}{\sigma^{\pm}}$$

$$\frac{\partial \phi_e}{\partial x}(x,t) = -\frac{i_e^{\pm}(x,t)}{\kappa} + \frac{2RT}{F} (1 - t_c^0)$$

$$\times \left(1 + \frac{d \ln f_{c/a}}{d \ln c_e}(x,t)\right) \frac{\partial \ln c_e}{\partial x}(x,t)$$
(18)

in which $k_f(x,t) := (1 + (d \ln f_{c/a})/(d \ln c_e)(x,t))$ is approximated as a constant parameter in x, i.e., $\overline{k}_f \approx k_f(x,t)$, $\forall x \in [0^-, 0^+]$. Moreover, the ionic current density in the electrolyte phase, i_e^{\pm} , may be forthrightly determined by the spatially uniform current density (see, e.g., [18, Fig. 3]).

The output voltage of the cell, V(t), is measured across the current collectors

$$V(t) = \phi_s^+(0^+, t) - \phi_s^-(0^-, t)$$

$$= \left[\phi_e(0^+, t) - \phi_e(0^-, t)\right] + F\left[R_f^+ j_n^+(t) - R_f^- j_n^-(t)\right]$$

$$+ \left[\eta^+(t) - \eta^-(t)\right] + \left[U^+\left(c_{ss}^+(t)\right) - U^-\left(c_{ss}^-(t)\right)\right].$$
(19)

Assuming $\alpha = 0.5$ [18], [56], [57] and inverting the Butler–Volmer equation (6) yield the analytic expression for the overpotentials

$$\eta^{\pm}(t) = \frac{RT}{\alpha F} \sinh^{-1} \left[\frac{\mp I(t)}{2a^{\pm}L^{\pm}i_0^{\pm}(t)} \right]. \tag{20}$$

Note that $\alpha=0.5$ is a common assumption in the literature and has been proven to be almost always true in practice [18], [56], [57]. The electrolyte potential difference across current collectors, $\Delta \phi_e(t) = \phi_e(0^+,t) - \phi_e(0^-,t)$, can be computed by integrating equation (18) across the cell thickness

$$\Delta \phi_e(t) = \int_{0^-}^{0^+} -\frac{i_e^{\pm}(x,t)}{\kappa} dx + \frac{2RT}{F} (1 - t_c^0) \overline{k}_f \int_{0^-}^{0^+} \frac{\partial \ln c_e}{\partial x}(x,t) dx = -\frac{L^+ + 2L^{\text{sep}} + L^-}{2\kappa} I(t) + k_c \ln \left[\frac{c_e^+(0^+,t)}{c_e^-(0^-,t)} \right]$$
(21)

where $k_c := (2RT/F)(1 - t_c^0)\overline{k}_f$. Now, we combine (8) with (19)–(21) to compute cell voltage

$$V(t) = \frac{RT}{\alpha F} \sinh^{-1} \left[\frac{-I(t)}{2a^{+}AL^{+}i_{0}^{+}(t)} \right]$$

$$-\frac{RT}{\alpha F} \sinh^{-1} \left[\frac{I(t)}{2a^{-}AL^{-}i_{0}^{-}(t)} \right]$$

$$+U^{+}(c_{ss}^{+}(t)) - U^{-}(c_{ss}^{-}(t))$$

$$-\left(\frac{R_{f}^{+}}{a^{+}AL^{+}} + \frac{R_{f}^{-}}{a^{-}AL^{-}} \right) I(t)$$

$$-\frac{L^{+} + 2L^{\text{sep}} + L^{-}}{2\kappa} I(t)$$

$$+k_{f} \left[\ln c_{s}^{+}(0^{+}, t) - \ln c_{s}^{-}(0^{-}, t) \right]$$
 (22)

where $U^+(\cdot)$ and $U^-(\cdot)$ denote OCPs of two electrodes.

The key differences with respect to the existing SPMe model in [18] and [60] are underlined here. In [18] and [60], the values of exchange current density i_0^{\pm} , electrolyte conductivity κ , and electrolyte activity coefficient $f_{c/a}$ are nonlinear functions of volume-averaged electrolyte concentrations in each cell domain. The model we use, in contrast, assumes that these quantities are functions of electrolyte concentrations at the domain boundaries (see the exchange current density equation (7) for an example). This adjustment produces a voltage output function, (22), that is only dependent on the boundary values of solid phase and electrolyte phase dynamics, i.e., $c_{ss}^+(t), c_{ss}^-(t), c_e^-(0^-, t)$, and $c_e^+(0^+, t)$. As we will demonstrate in the following, this model enables a state observability analysis and a provably convergent state observer design in a feedback fashion. Let us denote SPMe in [18] and [60] as

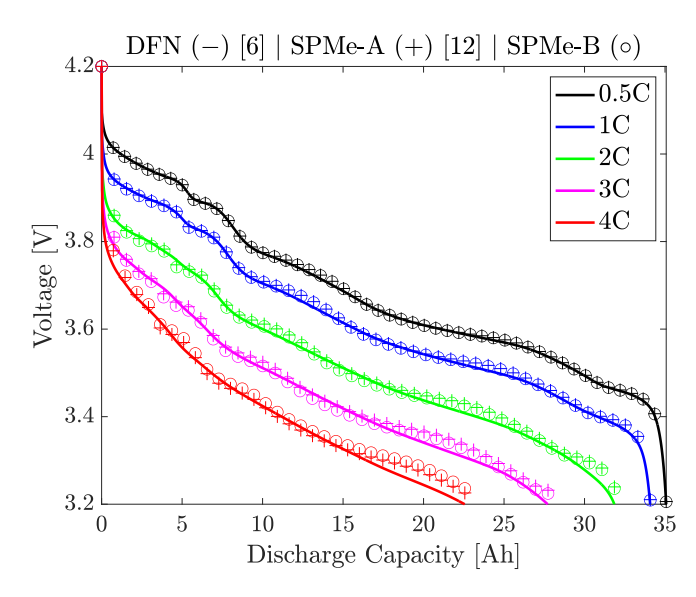


Fig. 2. Discharge curves at various C-rates for DFN model [10], SPMe-A [18], and SPMe-B.

"SPMe-A" (where "A" stands for average) and SPMe used in this article as "SPMe-B" (in which "B" stands for boundary) for the ease of presentation.

Remark 1 (Limitations of SPM Family): The assumption behind the SPM-based models is that the nonuniformity along the thickness of a battery is neglected. This nonuniformity can affect the prediction of uneven film growth and lithium plating [59]. One may choose to model the nonuniformity to achieve more granular modeling and analysis. However, in this work, our goal is to quantify lithium concentrations to a certain point and link it to battery SOH. This objective contrasts with having a physical insight of nonuniform side reaction mechanisms, which would require more descriptive physics-based degradation models and challenge the real-time applicability of the method.

B. Model Comparison

We numerically compare the open-loop voltage responses between SPMe-A, SPMe-B, and DFN models. The parameters of these three models are adopted from [18] and [62] for a lithium cobalt oxide (LCO) cathode. All three models are subject to the same set of parameters for consistency. Fig. 2 shows the discharge curves in terms of voltage at various constant C-rates, ranging from 0.5C to 4C. At low C-rates (<1C), both SPMe models exhibit accurate voltage predictions compared to DFN, as the electrolyte concentration gradient is relatively small across the spatial domain so that the boundary values of the electrolyte phase concentrations are close to the volume-averaged ones. Under high C-rates (>2C), as the electrolyte concentration gradient builds up, although SPMe model predictions slightly deviate from DFN, they offer decent approximations. Ultimately, the prediction accuracy in terms of root-mean-squared errors (RMSEs) between the two SPMe models and DFN is enumerated in Table II. Notably, SPMe-B consistently outperforms SPMe-A for current rates less than 4C. These results justify the utilization of boundary values

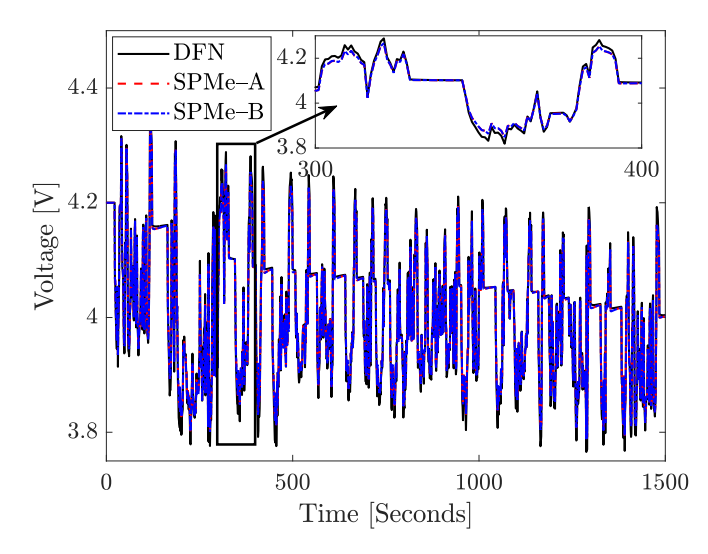


Fig. 3. Voltage prediction comparison of DFN model [10], SPMe-A [18], and SPMe-B on an FUDS cycle.

 $\label{eq:table_in_table} \textsc{Table II}$ RMSE Between SPMe and DFN

	0.5C	1C	2C	3C	4C	FUDS
SPMe-A	4 mV	7 mV	13 mV	14 mV	16 mV	10 mV
SPMe-B	3 mV	6 mV	11 mV	12 mV	21 mV	10 mV

of electrolyte phase concentration in the SPMe model for practical applications, even under high-current fast charging scenarios. Furthermore, voltage responses under a dynamic charge and discharge cycle, produced from a Federal Urban Driving Schedule (FUDS) [61], are shown in Fig. 3. The maximum C-rate is 3.3C and the mean C-rate is 0.4C. Both SPMe models predict voltage with a 10-mV RMSE. Consequently, hereafter, SPMe-B will be regarded as the plant model for state observability analysis and state/parameter estimation algorithm design.

III. STATE OBSERVABILITY ANALYSIS

We perform a state observability analysis for the SPMe model in the linear sense via frequency-domain model reduction and Kalman decomposition in this section. This section answers the fundamental question of whether solid phase and electrolyte phase lithium concentrations can be inferred concurrently from current and voltage data in an online fashion.

A. Frequency-Domain Model Order Reduction

Since the solid phase diffusion dynamics (1)–(4) are linear PDEs for both electrodes, the solutions can be analytically solved. This produces transcendental transfer functions linking lithium concentrations at any point r along the radius and input current [62]

$$\frac{C_s^{\pm}(r,s)}{I(s)} = \frac{e^{\sqrt{\frac{s}{D_s^{\pm}}}(R_s^{\pm}-r)} \left(e^{2\sqrt{\frac{s}{D_s^{\pm}}}r} - 1\right) m^{\pm} \left(R_s^{\pm}\right)^2}{\left(1 + R_s^{\pm} \sqrt{\frac{s}{D_s^{\pm}}} + e^{2R_s^{\pm} \sqrt{\frac{s}{D_s^{\pm}}}} \left(R_s^{\pm} \sqrt{\frac{s}{D_s^{\pm}}} - 1\right)\right) r} \tag{23}$$

where $C_s^{\pm}(r,s) = \mathcal{L}[c_s(r,t)]$ and $m^{\pm} = \pm 1/(D_s^{\pm}Fa^{\pm}L^{\pm})$. $\mathcal{L}[\cdot]$ is the Laplace transform operator. However, the most crucial quantities are lithium concentration at surface of electrode particle c_{ss}^{\pm} and volume-averaged lithium concentration \bar{c}_s^{\pm}

$$\bar{c}_s^{\pm}(t) = \frac{1}{4/3\pi \left(R_s^{\pm}\right)^3} \int_0^{R_s^{\pm}} c_s^{\pm}(r,t) \left(4\pi r^2\right) dr. \tag{24}$$

Here, c_{ss}^{\pm} has a direct impact on battery output voltage [see (22)] and also plays a crucial role in the charge transfer transfer kinetics, and \bar{c}_s^{\pm} is used to indicate the SOC in the electrodes [16]. Now, the transfer function for the surface concentration c_{ss}^{\pm} can be obtained by setting $r = R_s^{\pm}$ in (23)

$$\frac{C_{ss}^{\pm}(s)}{I(s)} = \frac{\sinh\left(\sqrt{\frac{s}{D_s^{\pm}}}R_s^{\pm}\right)m^{\pm}R_s^{\pm}}{R_s^{\pm}\sqrt{\frac{s}{D_s^{\pm}}}\cosh\left(\sqrt{\frac{s}{D_s^{\pm}}}R_s^{\pm}\right) - \sinh\left(\sqrt{\frac{s}{D_s^{\pm}}}R_s^{\pm}\right)}$$
(25)

where $C_{ss}^{\pm}(s) = \mathcal{L}[c_{ss}(t)]$. One can also conveniently obtain the transfer function of the volume-averaged concentration by evaluating

$$\frac{\bar{C}_s^{\pm}(s)}{I(s)} = \frac{1}{4/3\pi \left(R_s^{\pm}\right)^3} \int_0^{R_s^{\pm}} \frac{c_s^{\pm}(r,s)}{U(s)} \left(4\pi r^2\right) dr = \frac{q^{\pm}}{s}$$
 (26)

where $\bar{C}_s^{\pm}(s) = \mathcal{L}[\bar{C}_s^{\pm}(t)]$ and $q^{\pm} = 3D_s^{\pm}m^{\pm}/R_s^{\pm}$. Note that the transfer function (26) for the volume-averaged concentration is an integrator. In the time domain, this corresponds to the Coulomb counting procedure.

According to (9)–(11), the dynamics in the electrolyte phase is governed by a set of parabolic diffusion PDEs with forced current inputs. We assume that electrolyte diffusivity D_e^j and electrolyte volume fraction ε_e^j are uniform across the spatial domains. This assumption may generate modeling uncertainty to a certain level, but it strikes a balance between model accuracy and mathematical simplicity. Hereafter, denote $D_e = D_e^j$ and $\varepsilon_e = \varepsilon_e^j$ for all $j \in \{+, -, \text{sep}\}$. Under this scenario, the Laplace transform of electrolyte dynamics (9)–(11) are given by

$$\frac{d^2 C_e^j(x,s)}{dx^2} - \frac{s}{D_e} C_e^j(x,s) \mp \beta^j I(s) = 0$$
 (27)

where $C_e^j(x,s) = \mathcal{L}[c_e^j(x,t)]$, $\beta^\pm = (1-t_c^0)/(D_e\varepsilon_eFAL^\pm)$, and $\beta^{\rm sep} = 0$. The Laplace transform of the matching boundary conditions (12)–(16) are not repeated here. For simplicity of the analytical calculation of the electrolyte phase transfer functions, we assume $L^- = 1/4L$ and $L^{\rm sep} = 3/20L$, where $L = L^- + L^{\rm sep} + L^+$ denotes battery thickness [16]. Any other selections of cell geometry do not fundamentally change the subsequent analysis and application of the transfer functions. Ultimately, solving ordinary differential equation (ODE) (27) together with the boundary conditions for positive and negative electrodes yields the analytic transfer functions between electrolyte concentrations and current at cell

terminals $x = 0^-$ and $x = 0^+$

$$\frac{C_e^-(0^-, s)}{I(s)} = \frac{\gamma^-}{s} - \frac{\gamma^- \sinh\left(\frac{3}{4}L\sqrt{\frac{s}{D_e}}\right) + \gamma^+ \sinh\left(\frac{3}{5}L\sqrt{\frac{s}{D_e}}\right)}{s \cdot \sinh\left(L\sqrt{\frac{s}{D_e}}\right)} \tag{28}$$

$$\frac{C_e^+(0^+, s)}{I(s)} = -\frac{\gamma^+}{s} + \frac{\gamma^- \sinh\left(\frac{1}{4}L\sqrt{\frac{s}{D_e}}\right) + \gamma^+ \sinh\left(\frac{2}{5}L\sqrt{\frac{s}{D_e}}\right)}{s \cdot \sinh\left(L\sqrt{\frac{s}{D_e}}\right)}$$
(29)

with $\gamma^{\pm} = (1 - t_c^0)/(\varepsilon_e FAL^{\pm})$. It should be noted that, similar to the solid phase, our focus in the electrolyte phase is restricted to transfer functions at the domain boundaries. This occurs because the cell voltage, in particular the electrolyte concentration overpotential, is a direct function of electrolyte phase concentration at the cell terminals (see the last term in (22) for details).

Next, we will employ the Padé approximation to reduce the orders of the aforementioned nonlinear transcendental transfer functions (25), (26), (28), and (29) derived from battery PDE dynamics, so as to produce linearized representations of the models and investigate the observability of the internal states from voltage measurement [63]. The Padé approximation technique has emerged as one of the common strategies to perform model reduction for the family of SPMs because it conveniently approximates any general transcendental transfer function G(s) as a proper ratio of two power series that naturally possess poles and zeros depending on system characteristics. Furthermore, the order of the approximation can be dictated by the tradeoff between computational burden and desired model accuracy. Previous work [16] highlighted that the solid phase diffusion dynamics can be sufficiently approximated by a third-order truncation in highly transient electric vehicle applications where 90% of the current signal power for the drive cycles is within frequencies less than 2.5 Hz. Let

$$\frac{C_s^{\pm}(r,s)}{I(s)} \approx G_s^{\pm}(s) := \frac{b_{s,1}^{\pm}s^2 + b_{s,2}^{\pm}s + b_{s,3}^{\pm}}{s^3 + a_{s,1}^{\pm}s^2 + a_{s,2}^{\pm}s + a_{s,3}^{\pm}}.$$
 (30)

Note that the linear transfer function $G_s^{\pm}(s)$ in (30) is strictly proper since the order of the numerator is less than the order of the denominator [62]. Given the approximation order, the polynomial coefficients are computed via the method of moment matching [64]. Another crucial property of the transcendental transfer functions (25), (26), (28), and (29) is that the solid and electrolyte phases all contain poles at the origin of the complex plane. This indicates that the SPMe dynamics are only marginally stable so that open-loop state observers will not guarantee proper state estimation convergence. As a result, the Padé approximations must preserve the zero poles inherited from the original transfer functions. Hence, we must have

TABLE III
COEFFICIENTS OF PADÉ APPROXIMATIONS

Regions	Parameters
Solid	$a_{s,1}^{\pm} = \frac{189D_s^{\pm}}{(R_s^{\pm})^2}, b_{s,1}^{\pm} = \frac{21D_s^{\pm}m^{\pm}}{R_s^{+}}$ $a_{s,2}^{\pm} = \frac{3465(D_s^{\pm})^2}{(R_s^{\pm})^4}, b_{s,2}^{\pm} = \frac{1260(D_s^{\pm})^2m^{\pm}}{(R_s^{\pm})^3}$ $a_{s,3}^{\pm} = 0, b_{s,3}^{\pm} = \frac{10395(D_s^{\pm})^3m^{\pm}}{(R_s^{\pm})^5}$ $a_{e,1}^{\pm} = \frac{1}{B_{e,2}^{\pm}}, b_{e,1}^{\pm} = \frac{A_{e,1}^{\pm}}{B_{e,2}^{\pm}}$
	$a_{s,3}^{\pm} = 0, b_{s,3}^{\pm} = \frac{10395(D_s^{\pm})^3 m^{\pm}}{(R_s^{\pm})^5}$
	$a_{e,1}^{\pm} = \frac{1}{B_{e,2}^{\pm}}, b_{e,1}^{\pm} = \frac{A_{e,1}^{\pm}}{B_{e,2}^{\pm}}$
	where
	$A_{e,1}^{+} = -L^{2} \frac{(\gamma^{-})^{2} + 13.222\gamma^{-}\gamma^{+} + 16.273(\gamma^{+})^{2}}{2}$
Electrolyte	$D_e(93.659\gamma^- + 134.269\gamma^+)$
Electrolyte	where $A_{e,1}^+ = -L^2 \frac{(\gamma^-)^2 + 13.222\gamma^-\gamma^+ + 16.273(\gamma^+)^2}{D_e(93.659\gamma^- + 134.269\gamma^+)}$ $B_{e,2}^+ = \frac{0.114\gamma^-L^2 + 0.156\gamma^+L^2}{\gamma^-D_e + 1.434\gamma^+D_e}$ $A_{e,1}^- = -L^2 \frac{(\gamma^-)^2 + 1.350\gamma^-\gamma^+ + 0.073(\gamma^+)^2}{D_e(13.017\gamma^- + 15.234\gamma^+)}$ $B_{e,2}^+ = \frac{0.089\gamma^-L^2 + 0.115\gamma^+L^2}{\gamma^-D_e + 1.170\gamma^+D_e}$
	$A_{e,1}^{-} = -L^2 \frac{(\gamma^{-})^2 + 1.350\gamma^{-}\gamma^{+} + 0.073(\gamma^{+})^2}{D_2(13.017\gamma^{-} + 15.234\gamma^{+})}$
	$0.089\gamma^{-1}L^{2} + 0.115\gamma^{+}L^{2}$
	$B_{e,2} = {\gamma^- D_e + 1.170 \gamma^+ D_e}$

 $a_{s,3}^{\pm}=0$, and the values of a_s 's and b_s 's are documented in Table III.

The Padé-approximated frequency-domain transfer function (30) can then be realized in time domain by a linear state-space representation via a third-order controllable canonical form [65] as follows:

$$\dot{x}_s^{\pm}(t) = A_s^{\pm} x_s^{\pm}(t) + B_s^{\pm} I(t) \tag{31}$$

$$c_{ss}^{\pm}(t) = H_{ss}^{\pm} x_s^{\pm}(t) \tag{32}$$

$$\bar{C}_s^{\pm}(t) = \bar{H}_s^{\pm} x_s^{\pm}(t) \tag{33}$$

where $x_s^+, x_s^- \in \mathbb{R}^{n_s}$ with $n_s = 3$, and

$$x_{s}^{\pm} = \begin{bmatrix} x_{s,1}^{\pm} \\ x_{s,2}^{\pm} \\ x_{s,3}^{\pm} \end{bmatrix}, \quad A_{s}^{\pm} = \begin{bmatrix} 0 & 1 & 0 \\ 0 & 0 & 1 \\ -a_{s,3}^{\pm} & -a_{s,2}^{\pm} & -a_{s,1}^{\pm} \end{bmatrix}, \quad B_{s}^{\pm} = \begin{bmatrix} 0 \\ 0 \\ 1 \end{bmatrix}$$

$$H_{ss}^{\pm} = \begin{bmatrix} b_{s,3}^{\pm} \\ b_{s,2}^{\pm} \end{bmatrix}^{\top}, \quad \bar{H}_{s}^{\pm} = \begin{bmatrix} q^{\pm}a_{s,2}^{\pm} \\ q^{\pm}a_{s,1}^{\pm} \\ a^{\pm} \end{bmatrix}^{\top}. \tag{34}$$

It is evident that A_s^{\pm} has a zero eigenvalue since the transfer function $G_s^{\pm}(s)$ has a pole at the origin in each electrode since $a_{s,3}^{\pm} = 0$. As a result, an open-loop state observer in the solid phase will not achieve asymptotic stability.

Next, we examine the electrolyte phase dynamics. Similar to the solid phase, we now utilize a second-order Padé approximation for the transcendental transfer functions (28) and (29)

$$\frac{C_e^{\pm}(0^{\pm}, s)}{I(s)} \approx G_e^{\pm}(s) := \frac{b_{e,1}^{\pm} s + b_{e,2}^{\pm}}{s^2 + a_{e,1}^{\pm} s + a_{e,2}^{\pm}}.$$
 (35)

As before, to conserve the zero poles in (28) and (29), let $a_{e,2}^{\pm}=0$. Interestingly, the moment matching procedure [64] produces $b_{e,2}^{\pm}=0$, which indicates that $G_e^{\pm}(s)$ allows common poles and zeros at the origin in the plant transfer function. In this scenario, although the integrator mode becomes unobservable, $c_e^{\pm}(0,t)$ will not directly depend on the integrator mode. This suggests that the zero and pole at the origin can be canceled to achieve minimal realization, and the remaining

modes are fully observable. Consequently, the Padé approximation in (35) can be reduced to first order. Hence, by computing the common denominator for $G_e^+(s)$ and $G_e^-(s)$, the controllable canonical form for a second-order Padé approximation of the electrolyte phase transfer functions (28) and (29) is written as

$$\dot{x}_e(t) = A_e x_e(t) + B_e I(t) \tag{36}$$

$$c_e^+(0^+, t) = H_e^+ x_e(t) (37)$$

$$c_e^-(0^-, t) = H_e^- x_e(t)$$
 (38)

where $x_e \in \mathbb{R}^{n_e}$ with $n_e = 2$ and

$$x_{e} = \begin{bmatrix} x_{e,1} \\ x_{e,2} \end{bmatrix}, \quad A_{e} = \begin{bmatrix} 0 & 1 \\ -a_{e,1}^{+} a_{e,1}^{-} & -(a_{e,1}^{+} + a_{e,1}^{-}) \end{bmatrix}, \quad B_{e} = \begin{bmatrix} 0 \\ 1 \end{bmatrix}$$

$$H_{e}^{+} = \begin{bmatrix} a_{e,1}^{-} b_{e,1}^{+} & b_{e,1}^{+} \end{bmatrix}, \quad H_{e}^{-} = \begin{bmatrix} a_{e,1}^{+} b_{e,1}^{-} & b_{e,1}^{-} \end{bmatrix}. \tag{39}$$

The coefficients in (39) can be found in Table III. Ultimately, the composite state-space representation of the solid phase dynamics with both electrodes, electrolyte phase dynamics, and the cell voltage is given by

$$\dot{x}(t) = Ax(t) + BI(t) \tag{40}$$

$$y(t) = h(x(t), I(t)) \tag{41}$$

where $x \in \mathbb{R}^N$ with $N = (2n_s + n_e)$ and

$$x = \begin{bmatrix} x_s^+ \\ x_s^- \\ x_e \end{bmatrix}, \quad A = \begin{bmatrix} A_s^+ & 0 & 0 \\ 0 & A_s^- & 0 \\ 0 & 0 & A_e \end{bmatrix}, \quad B = \begin{bmatrix} B_s^+ \\ B_s^- \\ B_e \end{bmatrix}. \quad (42)$$

The output function (41) represents cell voltage and is collectively characterized by (22), (32), (33), (37), and (38).

Remark 2: The zero-pole cancellation at the origin in the electrolyte phase is a crucial property for SPMe system observability because it naturally eliminates the unobservable modes. As a result, the system matrix A in (42) has two zero eigenvalues, one of which originates from the solid phase dynamics in the negative electrode and the other stems from the solid phase dynamics in the positive electrode.

B. Observability Decomposition

One of the core objectives is to study the state observability of the SPMe system containing dynamics of solid phase with both electrodes and electrolyte phase from current and voltage measurements, in a mathematically rigorous way. This is accomplished by adopting the concept of Kalman decomposition [66], [67]. A Kalman decomposition is a linear transformation that decouples a system based on the observability and controllability of the subspaces. It separates the state space into four distinct components: observable and controllable subspace, observable and uncontrollable subspace, unobservable and controllable subspace, and unobservable and uncontrollable subspace. The Kalman decomposition brings a system into a structure upon which the observable and controllable subspaces can be clearly identified. We now introduce this useful technique to facilitate the observability analysis and the subsequent observer designs.

Theorem 1 (Observability Decomposition [68]): Consider an *n*-dimensional unobservable linear time-invariant (LTI) system $\dot{x} = Ax + Bu$ and y = Cx + Du. Suppose that the rank

of the observability matrix, rank(\mathcal{O}), is d with d < n. Let P_o groups d linearly independent rows of \mathcal{O} and $P = [P_o \ P_{uo}]^{\top}$, where P_{uo} consists of randomly constructed rows to produce an invertible P. Then, the similarity transformation $\bar{x} = Px$ brings the LTI system to the following form:

$$\begin{bmatrix} \dot{\bar{x}}_o \\ \dot{\bar{x}}_{uo} \end{bmatrix} = \begin{bmatrix} \bar{A}_o & 0 \\ \bar{A}_{21} & \bar{A}_{uo} \end{bmatrix} \begin{bmatrix} \bar{x}_o \\ \bar{x}_{uo} \end{bmatrix} + \begin{bmatrix} \bar{B}_o \\ \bar{B}_{uo} \end{bmatrix} u, \quad \bar{x}_o \in \mathbb{R}^d \quad (43)$$
$$y = \begin{bmatrix} \bar{C}_o & 0 \end{bmatrix} \begin{bmatrix} \bar{x}_o \\ \bar{x}_{uo} \end{bmatrix} + Du. \quad (44)$$

Moreover, the pair (\bar{A}_o, \bar{C}_o) is observable.

Let the state space of \bar{x} and u be χ and \mathcal{U} , respectively. In (43), \bar{x}_o is the observable subspace, whereas \bar{x}_{uo} represents the unobservable subspace since the pair (\bar{A}_o, \bar{C}_o) is observable and \bar{x}_{uo} is not reflected in the output equation (44). As such, a convergent closed-loop state observer can be designed to estimate the \bar{x}_o subspace. However, if the matrix \bar{A}_{uo} for the unobservable subspace of the system is Hurwitz (this facilitates a detectable system), then a convergent open-loop observer for the unobservable state \bar{x}_{uo} may be constructed, but the convergence speed would be completely dictated by the eigenvalues of the matrix \bar{A}_{uo} . Next, we apply the observability decomposition to a linearized version of the nonlinear battery SPMe model (40) and (41).

C. SPMe Model Observability Analysis

This section answers the question of "can we estimate the entire state space of the SPMe model (40) and (41) using current and voltage measurements?" We study the local observability of the nonlinear reduced-order SPMe system via linearizing the voltage map (41). The Jacobian of function h(x, I) with respect to x can be computed via $C_p = dh/dx =$ $[\partial h/\partial x_s^+ \quad \partial h/\partial x_s^- \quad \partial h/\partial x_e]$. The first two terms in C_p involve $\partial U^{\pm}/\partial c_{ss}^{\pm}$, the slopes of the OCP curves. They play a crucial role in state observability as the OCP curve for negative electrode is typically flat in the mid-SOC region [32]. This flatness produces small numeric values for the gradient $\partial U^{-}/\partial c_{ss}^{-}$, which eventually weakens the local state observability. However, states in the SPMe model (40) will still not be locally observable even around regions with high OCP gradients since the pair (A, C_p) is inherently not observable. This is fundamentally caused by the zero poles in the solid phase dynamics, which is further stated in the following proposition.

Proposition 1 (Observability of Reduced-Order SPMe Model): The observability matrix \mathcal{O} is rank deficient, i.e., rank(\mathcal{O}) = N-1 around any equilibrium points in χ , that is, states of the SPMe system (40) and (41) are not locally observable from current and voltage.

The proof of Proposition 1 is straightforward by realizing $a_3^\pm=0$. At this moment, since the SPMe system is not locally observable, we are positioned to apply Theorem 1 to decouple the SPMe system (40) phase out the unobservable subspace. This procedure requires d=(N-1) linearly independent rows from the observability matrix \mathcal{O}_p . An intriguing property to highlight is that the matrix $\bar{A}_{uo}\equiv 0$ in spite of the choice of P_{uo} . Thus, the transformed system (43) and (44) based on the reduced-order SPMe model is not detectable—thus disallowing an asymptotically convergent open-loop observer

for the unobservable subspace. Our goal is to estimate the entire state space in the transformed domain and then reconstruct the critical lithium concentrations in the solid phase and the electrolyte phase. This cannot be accomplished without the knowledge of \bar{x}_{uo} . From the preceding discussions, since \bar{x}_{uo} may be dynamically estimated by neither an open-loop observer nor a closed-loop observer, we seek to explore the fundamental properties of an electrochemical battery system to purposely construct the state \bar{x}_{uo} such that it is known *a priori*. We present the following proposition, which elucidates the physical conservation of lithium inventory in the solid phase.

Proposition 2 (Conservation of Solid Phase Lithium): The inventory of solid phase lithium is conserved [18], [34]. This is $dn_{\text{Li},s}/dt = 0$ with

$$n_{\text{Li},s} = \sum_{j=\{+,-\}} \frac{\epsilon_s^j L^j A}{4/3\pi \left(R_s^j\right)^3} \int_0^{R_s^j} c_s^j(r,t) (4\pi r^2) dr$$
$$= \epsilon_s^+ L^+ A \bar{C}_s^+ + \epsilon_s^- L^- A \bar{C}_s^-. \tag{45}$$

Coincidentally, since $\bar{C}_s^{\pm} = \bar{H}_s^{\pm} x_s^{\pm}$ [see (33)], $n_{\text{Li},s}$ may be alternatively expressed as

$$n_{\text{Li},s} = \varepsilon_s^+ L^+ A \bar{H}_s^+ x_s^+ + \varepsilon_s^- L^- A \bar{H}_s^- x_s^- = \mathbf{M} x \tag{46}$$

where $\mathbf{M} = [\varepsilon_s^+ L^+ A \bar{H}_s^+ \quad \varepsilon_s^- L^- A \bar{H}_s^- \quad 0]$. Hence, by adopting the relation in (46), we may mathematically force $\bar{x}_{uo} = n_{Li,s}$ by making $P_{uo} = \mathbf{M}$. This construction produces a time-invariant \bar{x}_{uo} as follows:

$$\bar{x}_{uo} = P_{uo}x = \mathbf{M}x = n_{\text{Li},s}. \tag{47}$$

With an accurate knowledge of lithium inventory in the solid phase $n_{\text{Li},s}$, the state \bar{x}_{uo} becomes a constant. Therefore, despite the fact that \bar{x}_{uo} is not dynamically observable from system output voltage, its temporal evolution can be predetermined.

As per Proposition 1, the reason why SPMe model states are not fully locally observable is the zero columns in matrices A_s^+ and A_s^- from the solid phase dynamics (31). Namely, this stems from the poles at the origin in the solid phase surface concentration transfer functions in (25). Although the transfer functions for the electrolyte phase (28) and (29) also have poles at the origin, they are not the key contributing factor for the loss of observability in SPMe. This occurs because of the zero-pole cancellation at the origin in the Padé approximation of the electrolyte phase dynamics, as elucidated by Remark 2. Eventually, this unique property allows us to compensate for the observability deficiency using only one algebraic relation that, by construction, exploits the conservation of lithium feature in the solid phase.

Remark 3 (Observability Improvement With Thermal Dynamics): Previous works have demonstrated the improvement of lithium concentration state observability in an electrochemical model by exploiting the electrochemical—thermal coupling [31], [34]. This is because the thermal model brings additional information about the electrode surface concentrations and the additional temperature measurements enhance the awareness of battery status. Although the present work does not account for battery thermal effects, the

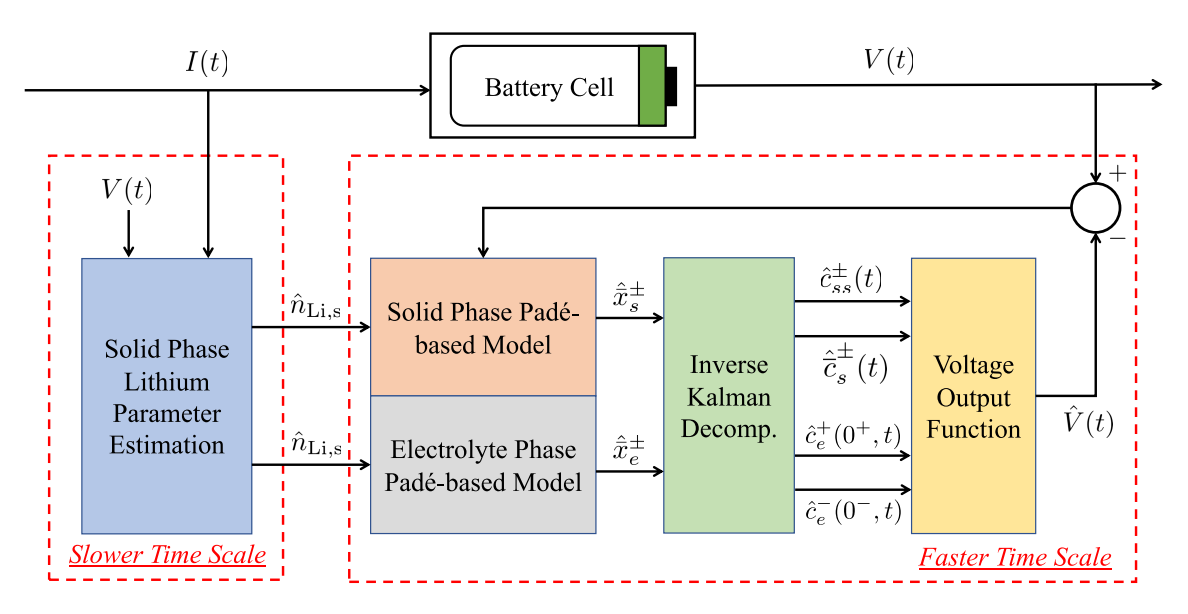


Fig. 4. Workflow of the SPMe state observer. It consists of the solid and electrolyte phase Padé-based estimator (coral and gray), inverse Kalman decomposition (green), and solid phase lithium estimator (blue). The observer produces estimates of solid phase and electrolyte phase lithium concentrations, as well as the inventory of solid phase lithium.

observability of an SPMe-thermal model is expected to be even stronger.

One practical issue associated with the aforementioned framework is that the total inventory of lithium in the solid phase, $n_{\text{Li},s}$, is not known beforehand and must be determined from data. It has been previously demonstrated in the literature that solid-electrolyte interphase (SEI) growth, among others, consumes cyclable lithium, which eventually causes cell charge capacity loss [69], [70]. Hence, $n_{\text{Li},s}$ will be slowly degrading over time as a result of unwanted side reactions. In Section IV, we will develop a sensitivity-based parameter estimation scheme to track the changes in solid phase lithium inventory to: 1) improve state observability and facilitate a state observer design and 2) quantify battery SOH.

A block diagram of the subsystems in this framework is shown in Fig. 4. A nonlinear state observer (to be proposed in Section V) based on the Padé-based reduced-order SPMe model in the transformed domain by the aforementioned Kalman decomposition produces estimates of solid phase and electrolyte phase lithium concentrations, enabled by the knowledge of total moles of solid phase lithium $n_{Li,s}$. A sensitivity-based parameter estimation algorithm for identifying $n_{Li,s}$ runs in parallel relying on battery voltage and current measurements. It is noteworthy that the estimation structure in Fig. 4 adopts the hierarchical multitime-scale strategy [71], [72] since the state estimation algorithms operate on a faster time scale (i.e., seconds), whereas the parameter identification scheme pilots on a much slower time scale (i.e., cycles). This is because the loss of lithium inventory is slow across a battery's life cycle [39] so that the changes in its values are refreshed less frequently.

IV. SENSITIVITY-BASED PARAMETER ESTIMATION

In this section, we aim to estimate the total moles of lithium in the solid phase, $n_{Li,s}$, also identified as the unobservable

state, \bar{x}_{uo} in Section III-C. Given the fact that the $n_{\text{Li},s}$ information is unknown, a sensitivity-based parameter estimation approach can provide the parameter estimates with statistical uncertainty bounds. This approach ultimately provides the unobservable state information, enabling state estimator designs.

First, we combine the SPMe model dynamics (1)–(22) with the algebraic equation (45), which results in an ODE system as follows:

$$\dot{x} = f(x, u), \quad x(t_0 \mid \theta) = x_0$$
 (48)

$$y = h(x, u), \quad y(t_0 \mid \theta) = y_0$$
 (49)

where $f(\cdot, \cdot)$ encodes the dynamical equations in the SPMe model and $h(\cdot, \cdot)$ denotes the output equation defined in (41). The states and inputs are denoted by $x \in \mathbb{R}^N$ and $u \in \mathbb{R}$, respectively. In this system, we note that the change of $\theta = n_{\text{Li},s}$ (or equivalently θ) only alters the initialization of the SPMe system, as shown by (48) and (49).

Next, the sensitivity dynamical system is derived to understand the relationship between output and parameter values [73]. Here, the local sensitivities of the output with respect to parameters are given by the first-order derivatives at the nominal parameter values. We now discuss the steps to derive the dynamical system of local sensitivity of $n_{\text{Li},s}$ in the SPMe model. First, let the sensitivity of the states and output with respect to θ be

$$S_x = \frac{\partial x}{\partial \theta}, \quad S_y = \frac{\partial y}{\partial \theta}.$$
 (50)

Moreover, $s_{i,j}$ is defined as the partial derivative of the *i*th state to the *j*th algebraic variable

$$s_{i,j}(t) = \frac{\partial x_i(t)}{\partial \theta_j}.$$
 (51)

Now, the sensitivity differential equations (SDEs) for the battery SPMe model (48) and (49) can be formulated as follows:

$$\dot{S}_x = \frac{\partial f}{\partial x} \cdot S_x + \frac{\partial f}{\partial \theta}, \quad S_x(t_0) = S_{x_0}$$
 (52)

$$S_y = \frac{\partial h}{\partial x} \cdot S_x + \frac{\partial h}{\partial \theta}, \quad S_y(t_0) = S_{y_0}$$
 (53)

where

$$1 = \frac{\partial f}{\partial x} \cdot S_x(t_0) + \frac{\partial f}{\partial \theta}$$

$$0 = \frac{\partial h}{\partial x} \cdot S_x(t_0) + \frac{\partial h}{\partial \theta}.$$
(54)

The first equation in (54) is obtained by computing the derivative of (46) with respect to $n_{\text{Li},s}$, and the second equation in (54) is the initial condition for voltage output equation. The initial conditions for sensitivity dynamical system are computed by solving these algebraic equations. It is worth highlighting that the above sensitivity dynamic equations are ODEs rather than differential algebraic equations. This can be attributed to the fact that the algebraic variable (54) only has an impact on the state initialization in (48). Subsequently, sensitivity equations will be integrated to minimize the voltage prediction in a nonlinear least-squares fashion, namely,

$$\min_{\hat{\theta}} \sum_{t=0}^{t_f} \left[y(t) - \hat{y}(t; \hat{\theta}) \right]^2. \tag{55}$$

To iteratively solve the optimization problem (55), we adopt the L-M algorithm [44], [74]. In essence, L-M adaptively switches the parameter update scheme between the gradient descent method and the Gauss–Newton method based on

$$\left[\mathbf{J}^{\mathsf{T}}\mathbf{J} + \lambda \operatorname{diag}(\mathbf{J}^{\mathsf{T}}\mathbf{J})\right] h_{\theta} = \mathbf{J}^{\mathsf{T}}(y - \hat{y})$$
 (56)

where $\mathbf{J}=\partial\hat{y}/\partial\hat{\theta}$ is the local sensitivity of the output \hat{y} , which is equivalent to the sensitivity vector computed from (52) to (54). λ trades off gradient descent update and Gauss–Newton update. Finally, the parameter estimates can be updated iteratively according to

$$\hat{\theta}_{k+1} = \hat{\theta}_k + h_{\hat{\theta}}.\tag{57}$$

Remark 4 (Convergence of L-M Algorithm): The L-M algorithm is essentially a numerical optimization algorithm for solving nonlinear systems, and thus, global convergence is generally not guaranteed. However, the convergence of L-M algorithm can be established under sets of specific convex constraints conditions, and we refer the interested readers to [78] and [79].

Remark 5 (Significance of $n_{\text{Li},s}$ Knowledge): The knowledge of $n_{\text{Li},s}$ obtained by the sensitivity-based parameter estimation not only facilitates SPMe state observability, as we have demonstrated in Section III, but also provides one of the most critical indicators for battery SOH/capacity degradation. Moreover, one can also estimate other critical aging parameters, e.g., film resistance and diffusion coefficients, using the L-M algorithm.

V. DESIGN OF NONLINEAR STATE OBSERVER

We now propose an asymptotically convergent state estimator to estimate the observable subspace \bar{x}_o within the transformed coordinate by the Kalman decomposition, from only voltage and current measurements.

First, the plant model of the observable subspace can be expressed by

$$\dot{\bar{x}}_o(t) = \bar{A}_o \bar{x}_o(t) + \bar{B}_o u(t) \tag{58}$$

$$y(t) = h(\bar{x}_o(t), \bar{x}_{uo}, u(t))$$
 (59)

where $\bar{x}_{uo} = n_{\text{Li},s}$, whose numerical value can be obtained by the sensitivity-based parameter identification algorithm described in Section IV. Provided the states from the transformed domain \bar{x}_o and \bar{x}_{uo} , the nonlinear output map h in (59) can then be alternatively expressed by

$$h = \frac{RT}{\alpha F} \sinh^{-1} \left[\frac{-I(t)}{2a^{+}AL^{+}i_{0}^{+}(\bar{x}_{o}, \bar{x}_{uo})} \right]$$

$$- \frac{RT}{\alpha F} \sinh^{-1} \left[\frac{I(t)}{2a^{-}AL^{-}i_{0}^{-}(\bar{x}_{o}, \bar{x}_{uo})} \right]$$

$$+ U^{+}(\bar{x}_{o}, \bar{x}_{uo}) - U^{-}(\bar{x}_{o}, \bar{x}_{uo})$$

$$- \left(\frac{R_{f}^{+}}{a^{+}AL^{+}} + \frac{R_{f}^{-}}{a^{-}AL^{-}} \right) I(t)$$

$$- \frac{L^{+} + 2L^{\text{sep}} + L^{-}}{2\kappa} I(t)$$

$$+ k_{c} \left[\ln(H_{e}^{+}x_{e}) - \ln(H_{e}^{-}x_{e}) \right].$$
(60)

Remark 6 (Lipschitz Continuity): Given accurate estimation of \bar{x}_{uo} from Section IV, the nonlinear output function h in (60) is Lipschitz continuous with respect to \bar{x}_o since h is continuously differentiable [77]. Mathematically, one of the popular strategies to determine a Lipschitz constant, although conservative, is to calculate the infinity norm of $\partial h/\partial \bar{x}_o$, i.e., $\gamma = \|\partial h/\partial \bar{x}_o\|_{\infty}$. With that

$$\left\| h\left(\bar{x}_{o}^{i}, \bar{x}_{\text{uo}}, u\right) - h\left(\bar{x}_{o}^{j}, \bar{x}_{\text{uo}}, u\right) \right\| \leq \gamma \left\| \bar{x}_{o}^{i} - \bar{x}_{o}^{j} \right\| \tag{61}$$

for all $u \in \mathcal{U}$ and any \bar{x}_o^i , $\bar{x}_o^j \in \chi$.

Now, we adopt a linear output error injection philosophy to propose a state observer for the nonlinear plant model (58) and (59) as follows:

$$\dot{\bar{x}}_o(t) = \bar{A}_o \hat{\bar{x}}_o(t) + \bar{B}_o u(t) + p[y(t) - \hat{y}(t)]$$
 (62)

$$\hat{\mathbf{y}}(t) = h(\hat{\bar{\mathbf{x}}}_o(t), \bar{\mathbf{x}}_{uo}, u(t)). \tag{63}$$

Specifically, \hat{x}_o denotes the state estimation. The observer gain p is a design tuning knob in order to ensure the stability and convergence of the state observer system. Theorem 2 dictates the sufficient conditions for observer convergence, which is extended from similar state estimation designs for Lipschitz nonlinear systems [29], [78].

Theorem 2 (Convergence of State Observer): The state estimation error $e(t) = \bar{x}_o(t) - \hat{\bar{x}}_o(t)$ asymptotically converges to zero, if there exists feasible solutions to the linear matrix inequalities

$$M_{1} := \begin{bmatrix} \bar{A}_{o}^{\top} R + R \bar{A}_{o} & -R \\ -R & 0 \end{bmatrix} \prec 0$$

$$M_{2} := \begin{bmatrix} \gamma^{2} p p^{\top} & 0 \\ 0 & -\mathbf{I} - K \end{bmatrix} \succeq 0$$
(64)

where $R = R^{\top} > 0$ and $S = S^{\top} > 0$ symmetric positive definite matrices.

Proof: The estimation error e(t) is governed by

$$\dot{e}(t) = \bar{A}_o e(t) - p\tilde{y}(t) \tag{65}$$

by taking the difference between (58) and (62). $\tilde{y}(t) = y(t) - \hat{y}(t)$ represents output error. We now analyze the stability of the error dynamics (65) by adopting the Lyapunov function candidate

$$W(t) = e^{\top}(t)Re(t), \quad R = R^{\top} > 0.$$
 (66)

Taking the derivative of W yields

$$\frac{dW}{dt} = \dot{e}^{\top} R e + e^{\top} R \dot{e}$$

$$= (\bar{A}e - p\tilde{y})^{\top} R e + e^{\top} R (\bar{A}e - p\tilde{y})$$

$$= e^{\top} (\bar{A}^{\top} R + R \bar{A}) e - (p\tilde{y})^{\top} R e - e^{\top} R (p\tilde{y})$$

$$= [e^{\top} z^{\top}] M_1 \begin{bmatrix} e \\ z \end{bmatrix} \tag{67}$$

in which $z := p\tilde{y}$. If one chooses R such that the $M_1 < 0$, then $\dot{W} < 0$. Next, according to Remark 6, the Lipschitz continuity condition on the output function y produces

$$\|\tilde{y}\| = \|y - \hat{y}\| \le \gamma \|e\|.$$
 (68)

We now apply the Cauchy–Schwarz inequality [29] to $z = p\tilde{y}$: $||z|| \le ||p|| ||\tilde{y}|| \le \gamma ||p|| ||e||$, which can be alternatively written in the vector form by squaring both sides

$$z^{\mathsf{T}}z < \gamma^2 p p^{\mathsf{T}} e^{\mathsf{T}} e. \tag{69}$$

A tuning term, K, can be added to (69) to form a linear matrix inequality (LMI)

$$z^{\mathsf{T}}z - e^{\mathsf{T}}(\gamma^2 p p^{\mathsf{T}})e - z^{\mathsf{T}}Kz \le 0 \tag{70}$$

and K > 0 is a freely assigned tuning parameter. Next, (70) can be rearranged in terms of a LMI

$$\begin{bmatrix} e^{\top} & z^{\top} \end{bmatrix} M_2 \begin{bmatrix} e \\ z \end{bmatrix} \succeq 0. \tag{71}$$

Hence, $\dot{W}(t) < 0$, or equivalently W(t), converges to zero asymptotically, if the matrix inequalities in (64) are satisfied and $R = R^{\top} > 0$, $K = K^{\top} > 0$.

Remark 7 (Future Work of State Observer): The present study tackles a state estimation design problem for a nonlinear reduced-order SPMe model. In particular, we estimate: 1) solid phase volume-averaged lithium concentration; 2) solid phase surface lithium concentration; and 3) electrolyte phase concentrations at battery terminals, using battery voltage and current measurements only. For SPMe model with quasi-linear electrolyte PDEs (9)–(11), one can subsequently design another set of observers to estimate electrolyte phase lithium concentration across battery thickness using the electrolyte concentration information at the terminals provided in this article, by adopting methods such as PDE backstepping [79]. This is a topic for future work.

VI. ALGORITHM VALIDATION

This section presents simulation studies and experimental validations to evaluate the performance of the proposed estimation methodology.

A. Simulation Results

We first present simulation-based algorithm validation to evaluate the effectiveness of the developed state and parameter estimators for the reduced-order SPMe model. The battery chemistry under consideration is the same as those used in Section II-B. The SPMe model (1)–(22) is regarded as the plant model and utilized to generate battery voltage and current data. All state and parameter estimates are randomly initialized at wrong values on purpose. Specifically, the true initial conditions are $c_{ss}^+(0)/c_{s,\text{max}}^+ = 0.5464$, $c_{ss}^-(0)/c_{s,\text{max}}^- = 0.8263$, $c_e^+(0^+, 0) = c_e^-(0^-, 0) = 2000 \text{ mol/m}^3$, and the corresponding initial cell voltage is V(0) = 4.0 V. With this, the total inventory of solid phase lithium is $n_{\text{Li},s} = 2.1329$ mol. This parameter will be recursively identified via the sensitivitybased L-M algorithm from Section IV. The state observer (62) and (63) is implemented numerically based on the observable \bar{x}_o -system (58) and (59), and the observer gains are selected according to the LMI condition (64) in Theorem 2. Furthermore, solid phase lithium concentrations are reported by their normalized values throughout this section, i.e., $\theta_{ss}^{\pm} = c_{ss}^{\pm}/c_{s,\text{max}}^{\pm}$ and $\bar{\theta}_s^{\pm} = \bar{c}_s^{\pm}/c_{s,\text{max}}^{\pm}$, and the electrolyte phase lithium concentrations are reported by the differences from the initial conditions, i.e., $\tilde{c}_e^{\pm}(0^{\pm}, t) = c_e^{\pm}(0^{\pm}, t) - c_e^{\pm}(0^{\pm}, 0)$.

1) Parameter Identification: From an electrochemical perspective, a decrease in total amount of $n_{Li,s}$ is considered as a way for battery degradation, which results in capacity fading. This is because many aging mechanisms and unwanted side reactions consume cyclable lithium. Consequently, over time, battery voltage responses will deviate from that of a fresh cell. Fig. 5(c) showcases the impact of $n_{Li,s}$ degradation on the trajectories of battery voltage, under the Urban Dynamometer Driving Schedule (UDDS) drive cycle. This input profile is also leveraged for the identification of parameter $n_{Li,s}$ since the highly transient profile produces a sufficiently rich signal. In the simulation validation, suppose that the battery under consideration has undergone considerable numbers of cycles to exhibit degradation, and the "true" (aged) value of parameter $n_{\text{Li},s}$ is set to $n_{\text{Li},s}^* = 2.1329$ mol. Furthermore, the initial guess in the parameter estimator is $\hat{n}_{\text{Li},s}(0) = 2.50$ mol. The estimated parameter is updated at the end of each iteration, which is plotted against the true parameter value in Fig. 5(a). We also observe from Fig. 5(a) and (b) that there are two plateaus during the parameter estimation procedure. This is due to the fact that the nonlinearity of the voltage function affects the parameter estimation results. To ensure parameter estimation convergence, the algorithm automatically halts when the voltage RMSE is less than 0.01 mV. Ultimately, the estimated parameter $\hat{n}_{\text{Li},s} = 2.1331 \text{ mol has less than } 0.01\%$ error with respect to the true value $n_{\text{Li.s}}^* = 2.1329 \text{ mol.}$

2) State Estimation: Given accurate estimation of total moles of solid phase lithium $\hat{n}_{\text{Li},s}$ from Section VI-A1, we evaluate the effectiveness of the proposed LMI-based state

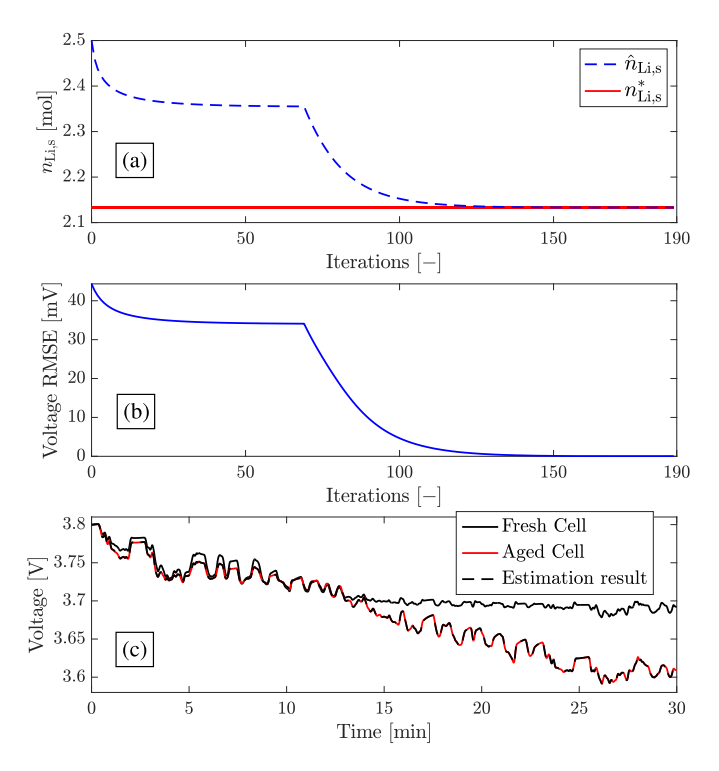


Fig. 5. Parameter identification results for solid phase lithium inventory $n_{\mathrm{Li},s}$ using a UDDS drive cycle. The voltage RMSE is reduced to less than 0.01 mV via the L-M algorithm. (a) $n_{\mathrm{Li},s}$ estimates. (b) Voltage estimate RMSE. (c) Effect of $n_{\mathrm{Li},s}$ degradation to voltage.

observer using the Kalman decomposition. Note again that, $n_{Li,s}$ degrades at a slower time scale, while the state estimation algorithm operates on a faster time scale. As a sanity check, we first consider a constant 1C discharge for 20 min, followed by a 10-min relaxation period. Fig. 6(a) visualizes the input current profile. The state observer's initial estimation errors are 10.5%, 20.9%, 5.5%, and 16.9% for $\hat{c}_{ss}^{+}(t)$, $\hat{c}_{ss}^{-}(t)$, $\hat{c}_{e}^{+}(0^{+}, t)$, and $\hat{c}_{\rho}^{-}(0^{-},t)$, respectively. As discussed in Section V, the state observer is designed and implemented in the transformed coordinate by the Kalman decomposition, and consequently, the convergence of lithium concentrations is shown in Fig. 6(b) and (c). The estimates of lithium concentrations asymptotically converge to the truth trajectories in less than 5 min with a proper selection of the observer gains. In addition, generally, the persistency of excitation (PE) for the parameter $n_{\text{Li},s}$ using a constant rate charging/discharging is not high enough to generate convergent parameter estimates [25]. This motivates the use of sufficiently rich UDDS cycle to identify the parameter in Section VI-A1, as well as testing the state observer using experimental data in Section VI-B.

B. Experimental Results

In this section, the performance of the proposed state and parameter estimation framework is evaluated via experimental data from an aged commercial lithium nickel-cobalt-aluminum oxide (NCA)—graphite cell. The experiments were carried out using Panasonic 2.7-Ah 18650 lithium NCA battery cells. The experimental setup consists of an Arbin LBT21084HC series battery tester with 0.02% full-scale

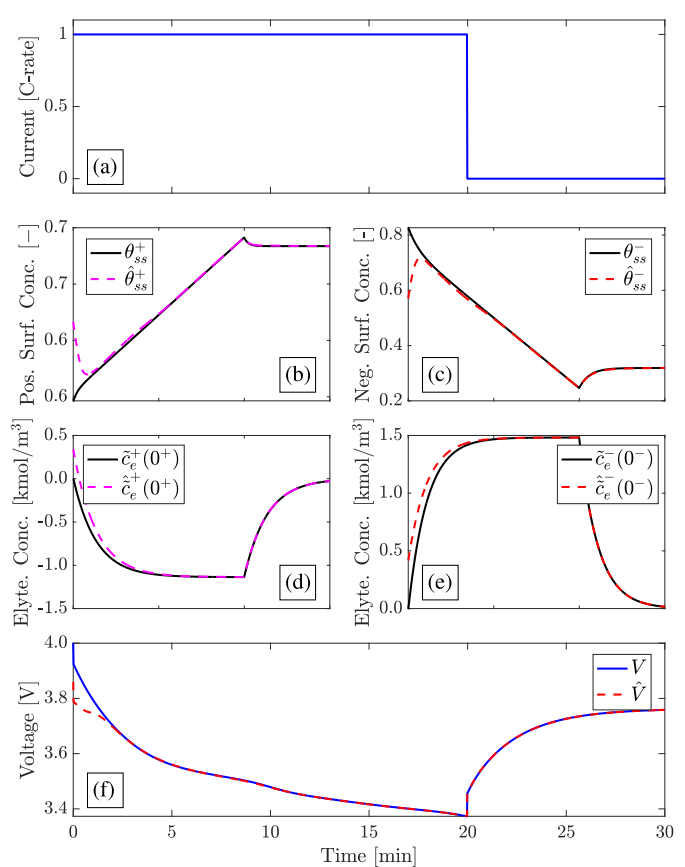


Fig. 6. State estimation results under a 30-min 1C constant discharge and relaxation. (a) Current profile. (b) Lithium surface concentration in positive electrode. (c) Lithium surface concentration in negative electrode. (d) Electrolyte lithium concentration at positive electrode terminal. (e) Electrolyte lithium concentration at negative electrode terminal. (f) Battery voltage.

range (FSR) accuracy. Battery measurements (current, voltage, and surface temperature) were collected each second. The experimentally collected current and voltage data, including OCV test, constant current charge and discharge, and drive cycles, have been utilized for parameterization of the SPMe model. For model identification, we adopt particle swarm optimization (PSO) that minimizes the root-mean-squared voltage error between experimental data and model to achieve the best model fit [80]. Specifically, we use the UDDS drive cycle data in Fig. 7(a) and (b) to perform experimental validations since it generates sufficiently rich information. The PSO-trained SPMe model generates less than 14-mV RMSE between the UDDS voltage data and the model output.

1) Parameter Identification: In this work, the total moles of solid phase lithium, $n_{\text{Li},s}$, is regarded as the primary battery aging parameter and will be recursively identified from the experimental data, that is, we assume that all other electrochemical parameters are known *a priori*, and the only parameter varying with battery degradation is $n_{\text{Li},s}$. Notably, although the focus of this study is to track $n_{\text{Li},s}$, the method can be universally adapted to estimating other degradation-related electrochemical parameters. We initialize the parameter estimate randomly at $\hat{n}_{\text{Li},s}(0) = 0.1638$ mol, which introduces an unreasonably high RMSE of 209 mV between

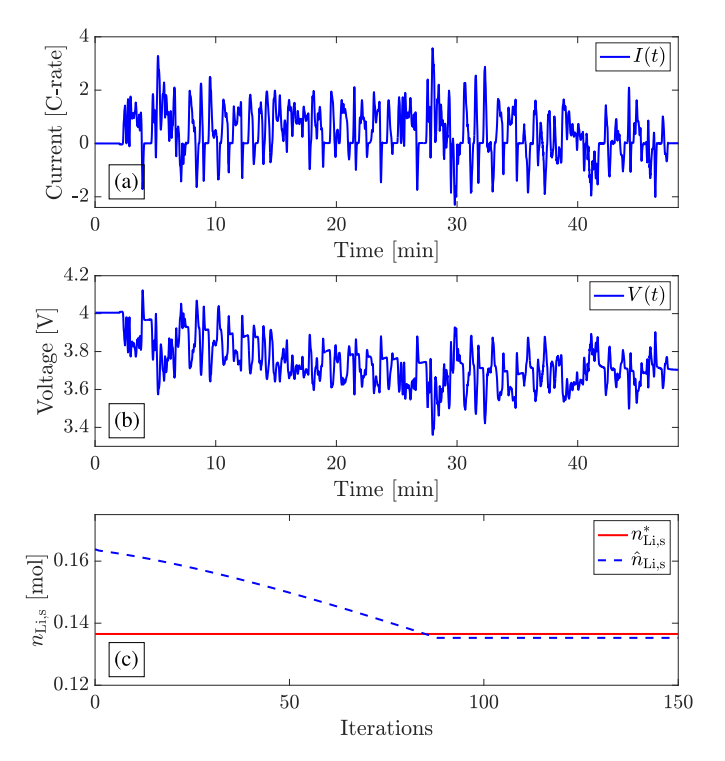


Fig. 7. Experimental parameter estimation results for a UDDS drive cycle. (a) Current. (b) Voltage. (c) $n_{\text{Li},s}$ estimation.

experimentally measured voltage and model-simulated voltage output. We then identify the moles of lithium by using the L-M algorithm in (56). The algorithm iterates the parameter updates until the voltage RMSE between the data and model drops below 14 mV, and the resultant estimation trajectory is shown in Fig. 7(c). Despite the fact that the $n_{\text{Li},s}$ estimate reaches the steady-state within 90 iterations, there exists a small bias (<1%). This uncertainty fundamentally stems from the model mismatch with experimental data. Note that in the simulation study in Section VI-A, we managed to achieve a voltage error less than 0.01 mV with the identified $\hat{n}_{\text{Li},s}$ since the modeling uncertainty was not present in the model-to-model validation. However, there inevitably are modeling uncertainties when it comes to experimental verification for the battery system, but the selected 14-mV cutoff voltage error is sufficient to produce a satisfactory $n_{Li,s}$ estimation performance with less than 1% error.

2) State Estimation: Next, with the knowledge of solid phase lithium inventory, we perform state estimation with the same electric vehicle charge/discharge cycle shown in Fig. 7(a). As discussed before, this dynamic cycle is highly transient whose mean and maximum C-rates are 0.39C and 3.57C, which are sufficiently significant to generate excitation to the electrolyte dynamics. In this case, the robustness of the state estimation algorithm will be challenged due to uncertainties in $\hat{n}_{\text{Li},s}$ estimates, i.e., $\hat{n}_{\text{Li},s} \approx 1.01 \cdot n_{\text{Li},s}^*$, and such uncertainties will propagate into the results of state estimation via (47). Besides, unlike simulation studies, we do not possess the knowledge of the true lithium concentration inside the battery. Consequently, the "truth" quantities will be produced via model simulation utilizing the identified parameters.

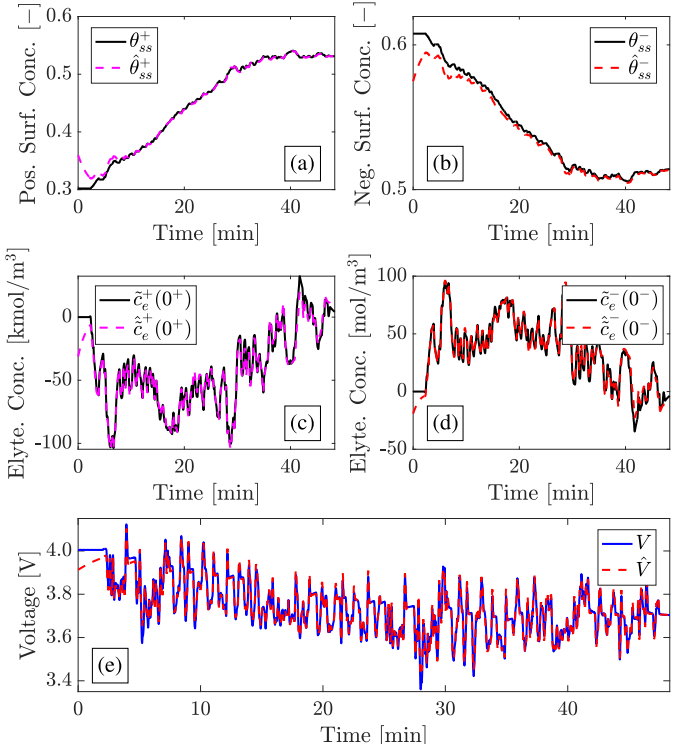


Fig. 8. Experimental state and voltage estimation results for a UDDS drive cycle. (a) Lithium surface concentration in the positive electrode. (b) Lithium surface concentration in the negative electrode. (c) Electrolyte lithium concentration at positive electrode terminal. (d) Electrolyte lithium concentration at negative electrode terminal. (e) Voltage.

The state observers are initialized with wrong values to validate the observer's convergence property. For the electrolyte phase concentration estimates in Fig. 8(c) and (d), after the initial transient (roughly 120 s), the estimates successfully converge to the "truth" trajectory with negligible disturbances caused by my model mismatch. As for the solid phase concentration estimates in Fig. 8(a) and (b), the estimation trajectories evolve with a slower speed compared with that of the electrolyte estimates but eventually produce 0.31% and 0.66% root-mean-squared percentage error for positive and negative electrodes, respectively. Remarkably, we note that the estimates for lithium concentration in the negative electrode present a small estimation bias stemming from $n_{Li,s}$ estimation error, which can be observed in Fig. 8(b). However, note in Fig. 8(e) that the voltage estimation error is relatively low with RMSE 13.7 mV after the initial transient period (close to the identified model RMSE). This is because the state observers slightly underestimate the solid phase lithium concentrations in the negative electrode to yield an accurate voltage estimation given perturbed $n_{Li,s}$ estimate. These results emphasize the importance of having accurate estimation of $n_{Li,s}$ in order to obtain the correct internal states as battery undergoes degradation.

3) Practical Considerations: The proposed methodology can be adopted by applications that require battery monitoring, control, and management, e.g., power electronics, electric vehicles, and stationary energy storage. Compared with an

ECM-based BMS, an electrochemical model-based framework will rigorously monitor lithium concentrations, potentials, and cyclable lithium inventory in a mathematically guaranteed fashion. This information is critical to the performance, safety, and longevity of batteries and can be leveraged as essential inputs to design battery physics-based fast and safe charging protocols. One practical universally recognized limitation is the proper parameterization of SPMe. Electrochemical models are characterized by many parameters, which may vary according to temperature, SOC, and health, and accurate parameterization of these (potentially weakly identifiable) parameters still remains a challenging topic. To mitigate this issue, prior studies have identified several solutions to improve parameter identifiability and convergence of identification algorithms [73], [81], [82].

VII. CONCLUSION

Typical battery state estimators focus on rough indicators such as Coulomb counting for SOC and capacity/resistance for SOH. However, these indicators do not pinpoint the physical sources of degradation. This article presents a mathematically elegant way to reconstruct specific battery electrochemical information, including the electrode-level states, together with the electrolyte dynamics and amount of cyclable lithium. The considered SPMe model is approximated in the frequency domain by the Padé approximation. The locally unobservable linearized state-space realization is then decomposed by the Kalman decomposition, which permits us to identify a single unobservable state. The solid phase lithium inventory then facilitates a nonlinear state observer design by predefining the evolution of the unobservable subspace. However, this assumption is difficult to meet in practice for battery manufacturers, and lithium inventory changes with battery aging. To counteract this, a sensitivity-based parameter estimation scheme is additionally developed to estimate lithium inventory as the battery degrades. The electrode-level solid phase and electrolyte phase states are crucial for battery charge and health monitoring, and this article rigorously identifies the unobservable components as well as the strategy to utilize only the solid phase lithium inventory to achieve mathematically guaranteed estimation in both solid and electrolyte phases.

REFERENCES

- N. A. Chaturvedi, R. Klein, J. Christensen, J. Ahmed, and A. Kojic, "Algorithms for advanced battery-management systems," *IEEE Control Syst. Mag.*, vol. 30, no. 3, pp. 49–68, Jun. 2010.
- [2] D. Zhang, S. Dey, H. E. Perez, and S. J. Moura, "Real-time capacity estimation of lithium-ion batteries utilizing thermal dynamics," *IEEE Trans. Control Syst. Technol.*, vol. 28, no. 3, pp. 992–1000, 2019.
- [3] M. A. Hannan, M. S. H. Lipu, A. Hussain, and A. Mohamed, "A review of lithium-ion battery state of charge estimation and management system in electric vehicle applications: Challenges and recommendations," *Renew. Sustain. Energy Rev.*, vol. 78, pp. 834–854, Oct. 2017.
- [4] L. Zhou, Y. Zhao, D. Li, and Z. Wang, "State-of-health estimation for LiFePO₄ battery system on real-world electric vehicles considering aging stage," *IEEE Trans. Transport. Electrific.*, vol. 8, no. 2, pp. 1724–1733, Jun. 2021.
- [5] L. Chen et al., "Online estimating state of health of lithium-ion batteries using hierarchical extreme learning machine," *IEEE Trans. Transport. Electrific.*, vol. 8, no. 1, pp. 965–975, Mar. 2022.

- [6] Z. Wang, C. Yuan, and X. Li, "Lithium battery state-of-health estimation via differential thermal voltammetry with Gaussian process regression," *IEEE Trans. Transport. Electrific.*, vol. 7, no. 1, pp. 16–25, Mar. 2021.
- [7] D. Zhang, S. Dey, H. E. Perez, and S. J. Moura, "Remaining useful life estimation of lithium-ion batteries based on thermal dynamics," in *Proc. Amer. Control Conf. (ACC)*, May 2017, pp. 4042–4047.
- [8] X. Hu, K. Zhang, K. Liu, X. Lin, S. Dey, and S. Onori, "Advanced fault diagnosis for lithium-ion battery systems: A review of fault mechanisms, fault features, and diagnosis procedures," *IEEE Ind. Electron. Mag.*, vol. 14, no. 3, pp. 65–91, Sep. 2020.
- [9] X. Hu, S. Li, and H. Peng, "A comparative study of equivalent circuit models for Li-ion batteries," *J. Power Sources*, vol. 198, pp. 359–367, Jan. 2015.
- [10] M. Doyle, T. F. Fuller, and J. Newman, "Modeling of galvanostatic charge and discharge of the lithium/polymer/insertion cell," *J. Elec-trochem. Soc.*, vol. 140, no. 6, pp. 1526–1533, Jun. 1993.
- [11] Y. Li, Z. Wei, B. Xiong, and D. M. Vilathgamuwa, "Adaptive ensemble-based electrochemical-thermal degradation state estimation of lithium-ion batteries," *IEEE Trans. Ind. Electron.*, vol. 69, no. 7, pp. 6984–6996, Jul. 2021.
- [12] G. K. Prasad and C. D. Rahn, "Development of a first principles equivalent circuit model for a lithium ion battery," in *Proc. Dyn. Syst. Control Conf.*, vol. 45301. New York, NY, USA: American Society of Mechanical Engineers, 2012, pp. 369–375.
- [13] G. Ning and B. N. Popov, "Cycle life modeling of lithium-ion batteries," J. Electrochem. Soc., vol. 151, no. 10, pp. A1584–A1591, 2004.
- [14] S. Santhanagopalan, Q. Guo, P. Ramadass, and R. E. White, "Review of models for predicting the cycling performance of lithium ion batteries," *J. Power Sources*, vol. 156, no. 2, pp. 620–628, 2006.
- [15] E. Prada, D. Di Domenico, Y. Creff, J. Bernard, V. Sauvant-Moynot, and F. Huet, "A simplified electrochemical and thermal aging model of LiFePO₄-graphite Li-ion batteries: Power and capacity fade simulations," *J. Electrochem. Soc.*, vol. 160, no. 4, pp. A616–A628, 2013.
- [16] J. Marcicki, M. Canova, A. T. Conlisk, and G. Rizzoni, "Design and parametrization analysis of a reduced-order electrochemical model of graphite/LiFePO₄ cells for SOC/SOH estimation," *J. Power Sources*, vol. 237, pp. 310–324, Sep. 2013.
- [17] T. R. Tanim, C. D. Rahn, and C.-Y. Wang, "State of charge estimation of a lithium ion cell based on a temperature dependent and electrolyte enhanced single particle model," *Energy*, vol. 80, pp. 731–739, Feb. 2015.
- [18] S. J. Moura, F. B. Argomedo, R. Klein, A. Mirtabatabaei, and M. Krstic, "Battery state estimation for a single particle model with electrolyte dynamics," *IEEE Trans. Control Syst. Technol.*, vol. 25, no. 2, pp. 453–468, Mar. 2017.
- [19] S. G. Marquis, V. Sulzer, R. Timms, C. P. Please, and S. J. Chapman, "An asymptotic derivation of a single particle model with electrolyte," *J. Electrochem. Soc.*, vol. 166, no. 15, pp. A3693–A3706, 2019.
- [20] P. Ramadass, B. Haran, R. White, and B. N. Popov, "Mathematical modeling of the capacity fade of Li-ion cells," *J. Power Sources*, vol. 123, no. 2, pp. 230–240, 2003.
- [21] G. L. Plett, "Algebraic solution for modeling SEI layer growth," *ECS Electrochemistry Lett.*, vol. 2, no. 7, pp. A63–A65, Apr. 2013.
- [22] T. R. Tanim and C. D. Rahn, "Aging formula for lithium ion batteries with solid electrolyte interphase layer growth," *J. Power Sources*, vol. 294, pp. 239–247, Oct. 2015.
- [23] D. Zhang, S. Dey, L. D. Couto, and S. J. Moura, "Battery adaptive observer for a single-particle model with intercalation-induced stress," *IEEE Trans. Control Syst. Technol.*, vol. 28, no. 4, pp. 1363–1377, Jul. 2020.
- [24] D. Di Domenico, A. Stefanopoulou, and G. Fiengo, "Lithium-ion battery state of charge and critical surface charge estimation using an electrochemical model-based extended Kalman filter," *J. Dyn. Syst., Meas.*, *Control*, vol. 132, no. 6, pp. 061302.1–061302.11, 2010.
- [25] S. J. Moura, N. Chaturvedi, and M. Krstic, "Adaptive PDE observer for battery SOC/SOH estimation," in *Proc. ASME Dyn. Syst. Control Conf.*, 2012, pp. 101–110.
- [26] S. J. Moura, N. A. Chaturvedi, and M. Krstić, "Adaptive partial differential equation observer for battery state-of-charge/state-of-health estimation via an electrochemical model," J. Dyn. Syst., Meas., Control, vol. 136, no. 1, Jan. 2014, Art. no. 011015.
- [27] A. Bartlett, J. Marcicki, S. Onori, G. Rizzoni, X. G. Yang, and T. Miller, "Electrochemical model-based state of charge and capacity estimation for a composite electrode lithium-ion battery," *IEEE Trans. Control Syst. Technol.*, vol. 24, no. 2, pp. 384–399, Mar. 2016.

- [28] D. Zhang, S. Dey, and S. J. Moura, "Lithium-ion battery state estimation for a single particle model with intercalation-induced stress," in *Proc. Annu. Amer. Control Conf. (ACC)*, Jun. 2018, pp. 2294–2299.
- [29] S. Dey, B. Ayalew, and P. Pisu, "Nonlinear robust observers for state-of-charge estimation of lithium-ion cells based on a reduced electro-chemical model," *IEEE Trans. Control Syst. Technol.*, vol. 23, no. 5, pp. 1935–1942, Sep. 2015.
- [30] R. Hausbrand et al., "Fundamental degradation mechanisms of layered oxide Li-ion battery cathode materials: Methodology, insights and novel approaches," Mater. Sci. Eng., B, vol. 192, pp. 3–25, Feb. 2015.
- [31] S. Dey and B. Ayalew, "Real-time estimation of lithium-ion concentration in both electrodes of a lithium-ion battery cell utilizing electrochemical-thermal coupling," J. Dyn. Syst., Meas., Control, vol. 139, no. 3, pp. 031007–031010, Mar. 2017.
- [32] A. Allam and S. Onori, "An interconnected observer for concurrent estimation of bulk and surface concentration in the cathode and anode of a lithium-ion battery," *IEEE Trans. Ind. Electron.*, vol. 65, no. 9, pp. 7311–7321, Sep. 2018.
- [33] S. Sattarzadeh, S. Dey, A. Colclasure, and K. Smith, "Addressing the observability problem in batteries: Algorithm design for electrode-level charge and health estimation," in *Proc. Amer. Control Conf. (ACC)*, Jul. 2020, pp. 1131–1136.
- [34] R. Klein, N. A. Chaturvedi, J. Christensen, J. Ahmed, R. Findeisen, and A. Kojic, "Electrochemical model based observer design for a lithium-ion battery," *IEEE Trans. Control Syst. Technol.*, vol. 21, no. 2, pp. 289–301, Mar. 2013.
- [35] B. Suthar et al., "Optimal control and state estimation of lithium-ion batteries using reformulated models," in *Proc. Amer. Control Conf.*, Jun. 2013, pp. 5350–5355.
- [36] R. B. Gopaluni and R. D. Braatz, "State of charge estimation in Liion batteries using an isothermal pseudo two-dimensional model," *IFAC Proc. Volumes*, vol. 46, no. 32, pp. 135–140, Dec. 2013.
- [37] A. M. Bizeray, S. Zhao, S. R. Duncan, and D. A. Howey, "Lithiumion battery thermal-electrochemical model-based state estimation using orthogonal collocation and a modified extended Kalman filter," *J. Power Sources*, vol. 296, pp. 400–412, Nov. 2015.
- [38] L. D. Couto and M. Kinnaert, "Internal and sensor fault detection and isolation for Li-ion batteries," *IFAC-PapersOnLine*, vol. 51, no. 24, pp. 1431–1438, 2018.
- [39] C. R. Birkl, M. R. Roberts, E. McTurk, P. G. Bruce, and D. A. Howey, "Degradation diagnostics for lithium ion cells," *J. Power Sources*, vol. 341, pp. 373–386, Feb. 2017.
- [40] M. Dubarry, V. Svoboda, R. Hwu, and B. Yann Liaw, "Incremental capacity analysis and close-to-equilibrium OCV measurements to quantify capacity fade in commercial rechargeable lithium batteries," *Electrochem. Solid-State Lett.*, vol. 9, no. 10, pp. A454–A457, 2006.
- [41] I. Bloom, J. Christophersen, and K. Gering, "Differential voltage analyses of high-power lithium-ion cells: 2. Applications," *J. Power Sources*, vol. 139, nos. 1–2, pp. 304–313, Jan. 2005.
- [42] X. Zhou, J. L. Stein, and T. Ersal, "Battery state of health monitoring by estimation of the number of cyclable Li-ions," *Control Eng. Pract.*, vol. 66, pp. 51–63, Sep. 2017.
- [43] M. Huang, M. Kumar, C. Yang, and A. Soderlund, Aging Estimation Lithium-Ion Battery Cell Using Electrochemical Model-Based Extended Kalman Filter. Reston, VA, USA: American Institute of Aeronautics and Astronautics, 2019, p. 0785.
- [44] S. Park, D. Zhang, R. Klein, and S. Moura, "Estimation of cyclable lithium for Li-ion battery state-of-health monitoring," in *Proc. Amer. Control Conf. (ACC)*, May 2021, pp. 3094–3101.
- [45] A. Bartlett, J. Marcicki, S. Onori, G. Rizzoni, X. Guang Yang, and T. Miller, "Model-based state of charge estimation and observability analysis of a composite electrode lithium-ion battery," in *Proc. 52nd IEEE Conf. Decis. Control*, Dec. 2013, pp. 7791–7796.
- [46] H. Fang, Y. Wang, Z. Sahinoglu, T. Wada, and S. Hara, "State of charge estimation for lithium-ion batteries: An adaptive approach," *Control Eng. Pract.*, vol. 25, pp. 45–54, Apr. 2014.
- [47] L. Wu, K. Liu, and H. Pang, "Evaluation and observability analysis of an improved reduced-order electrochemical model for lithium-ion battery," *Electrochimica Acta*, vol. 368, Feb. 2021, Art. no. 137604.
- [48] X. Li et al., "A physics-based fractional order model and state of energy estimation for lithium ion batteries. Part I: Model development and observability analysis," J. Power Sources, vol. 367, pp. 187–201, Nov. 2017.
- [49] D. Zhang, L. D. Couto, and S. J. Moura, "Electrode-level state estimation in lithium-ion batteries via Kalman decomposition," *IEEE Control Syst. Lett.*, vol. 5, no. 5, pp. 1657–1662, Nov. 2021.

- [50] K. E. Thomas, J. Newman, and R. M. Darling, "Mathematical modeling of lithium batteries," in *Advances in Lithium-Ion Batteries*. Cham, Switzerland: Springer, 2002, pp. 345–392.
- [51] E. Prada, D. Di Domenico, Y. Creff, J. Bernard, V. Sauvant-Moynot, and F. Huet, "Simplified electrochemical and thermal model of LiFePO₄graphite Li-ion batteries for fast charge applications," *J. Electrochem. Soc.*, vol. 159, no. 9, pp. A1508–A1519, 2012.
- [52] X. Han, M. Ouyang, L. Lu, and J. Li, "Simplification of physics-based electrochemical model for lithium ion battery on electric vehicle. Part I: Diffusion simplification and single particle model," *J. Power Sources*, vol. 278, pp. 802–813, Mar. 2015.
- [53] A. Nath, R. Mehta, R. Gupta, S. S. Bahga, A. Gupta, and S. Bhasin, "Control-oriented physics-based modeling and observer design for stateof-charge estimation of lithium-ion cells for high current applications," *IEEE Trans. Control Syst. Technol.*, early access, Mar. 11, 2022, doi: 10.1109/TCST.2022.3152446.
- [54] F. Lantelme, H. Groult, and N. Kumagai, "Study of the concentration-dependent diffusion in lithium batteries," *Electrochimica Acta*, vol. 45, no. 19, pp. 3171–3180, Jun. 2000.
- [55] L. O. Valøen and J. N. Reimers, "Transport properties of LiPF₆-based Liion battery electrolytes," *J. Electrochem. Soc.*, vol. 152, no. 5, p. A882, 2005
- [56] T. R. B. Grandjean, L. Li, M. X. Odio, and W. D. Widanage, "Global sensitivity analysis of the single particle lithium-ion battery model with electrolyte," in *Proc. IEEE Vehicle Power Propuls. Conf. (VPPC)*, Oct. 2019, pp. 1–7.
- [57] X. Hu, D. Cao, and B. Egardt, "Condition monitoring in advanced battery management systems: Moving horizon estimation using a reduced electrochemical model," *IEEE/ASME Trans. Mechatronics*, vol. 23, no. 1, pp. 167–178, Feb. 2018.
- [58] H. E. Perez, X. Hu, and S. J. Moura, "Optimal charging of batteries via a single particle model with electrolyte and thermal dynamics," in *Proc. Amer. Control Conf. (ACC)*, Jul. 2016, pp. 4000–4005.
- [59] X.-G. Yang and C.-Y. Wang, "Understanding the trilemma of fast charging, energy density and cycle life of lithium-ion batteries," *J. Power Sources*, vol. 402, pp. 489–498, Oct. 2018.
- [60] J. S. Newman. (2004). Fortran Programs for Simulation of Electrochemical Systems, Dualfoil. F Program for Lithium Battery Simulation. [Online]. Available: https://www.cchem.berkeley.edu/jsngrp/fortran.html
- [61] Y. Xing, W. He, M. Pecht, and K. L. Tsui, "State of charge estimation of lithium-ion batteries using the open-circuit voltage at various ambient temperatures," *Appl. Energy*, vol. 113, pp. 106–115, Jan. 2014.
- [62] J. C. Forman, S. Bashash, J. L. Stein, and H. K. Fathy, "Reduction of an electrochemistry-based Li-ion battery model via quasi-linearization and padé approximation," *J. Electrochem. Soc.*, vol. 158, no. 2, p. A93, 2010.
- [63] G. A. Baker, Jr., P. Graves-Morris, and S. S. Baker, *Padé Approximants: Encyclopedia of Mathematics and It's Applications*, vol. 59. Cambridge, U.K.: Cambridge Univ. Press, 1996.
- [64] A. C. Antoulas, Approximation of Large-Scale Dynamical Systems. Philadelphia, PA, USA: SIAM, 2005.
- [65] K. Ogata, Modern Control Engineering. Upper Saddle River, NJ, USA: Prentice-Hall, 2010.
- [66] H. Kimura, *Chain-Scattering Approach to H∞-Control*. Berlin, Germany: Springer, 2012.
- [67] L. Weiss and R. E. Kalman, "Contributions to linear system theory," Int. J. Eng. Sci., vol. 3, no. 2, pp. 141–171, Jul. 1965.
- [68] R. E. Kalman, "Mathematical description of linear dynamical systems," J. Soc. Ind. Appl. Math. A Control, vol. 1, no. 2, pp. 152–192, 1963.
- [69] X. Lin, J. Park, L. Liu, Y. Lee, A. M. Sastry, and W. Lu, "A comprehensive capacity fade model and analysis for Li-ion batteries," *J. Electrochem. Soc.*, vol. 160, no. 10, pp. A1701–A1710, 2013.
- [70] J. Christensen and J. Newman, "Effect of anode film resistance on the charge/discharge capacity of a lithium-ion battery," *J. Electrochem. Soc.*, vol. 150, no. 11, p. A1416, 2003.
- [71] C. Hu, B. D. Youn, and J. Chung, "A multiscale framework with extended Kalman filter for lithium-ion battery SOC and capacity estimation," *Appl. Energy*, vol. 92, pp. 694–704, Apr. 2012.
- [72] Y. Zou, X. Hu, H. Ma, and S. E. Li, "Combined state of charge and state of health estimation over lithium-ion battery cell cycle lifespan for electric vehicles," *J. Power Sources*, vol. 273, pp. 793–803, Jan. 2015.
- [73] S. Park, D. Kato, Z. Gima, R. Klein, and S. Moura, "Optimal experimental design for parameterization of an electrochemical lithium-ion battery model," *J. Electrochem. Soc.*, vol. 165, no. 7, pp. A1309–A1323, 2018.
- [74] K. Levenberg, "A method for the solution of certain non-linear problems in least squares," *Quart. J. Appl. Math.*, vol. 2, no. 2, pp. 164–168, Jul. 1944.

- [75] H. Dan, N. Yamashita, and M. Fukushima, "Convergence properties of the inexact Levenberg–Marquardt method under local error bound conditions," *Optim. Methods Softw.*, vol. 17, no. 4, pp. 605–626, Jan. 2002.
- [76] C. Kanzow, N. Yamashita, and M. Fukushima, "Levenberg–Marquardt methods with strong local convergence properties for solving nonlinear equations with convex constraints," *J. Comput. Appl. Math.*, vol. 172, no. 2, pp. 375–397, 2004.
- [77] H. J. Marquez, Nonlinear Control Systems. Hoboken, NJ, USA: Wiley, 2003.
- [78] R. Rajamani, "Observers for Lipschitz nonlinear systems," *IEEE Trans. Autom. Control*, vol. 43, no. 3, pp. 397–401, Mar. 1998.
- [79] M. Krstic and A. Smyshlyaev, Boundary Control of PDEs: A Course on Backstepping Designs. Philadelphia, PA, USA: SIAM, 2008.
- [80] S. Ebbesen, P. Kiwitz, and L. Guzzella, "A generic particle swarm optimization Matlab function," in *Proc. Amer. Control Conf. (ACC)*, Jun. 2012, pp. 1519–1524.
- [81] A. M. Bizeray, J.-H. Kim, S. R. Duncan, and D. A. Howey, "Identifiability and parameter estimation of the single particle lithium-ion battery model," *IEEE Trans. Control Syst. Technol.*, vol. 27, no. 5, pp. 1862–1877, Sep. 2019.
- [82] H. Pang, L. Mou, L. Guo, and F. Zhang, "Parameter identification and systematic validation of an enhanced single-particle model with aging degradation physics for Li-ion batteries," *Electrochimica Acta*, vol. 307, pp. 474–487, Jun. 2019.



Dong Zhang received the B.S. degree in civil and environmental engineering from the University of Michigan, Ann Arbor, MI, USA, in 2015, the B.S. degree in electrical and computer engineering from Shanghai Jiao Tong University, Shanghai, China in 2015, and the M.S. and Ph.D. degrees in systems and control engineering from the University of California at Berkeley, Berkeley, CA, USA, in 2016 and 2020, respectively.

He is currently an Assistant Professor in aerospace and mechanical engineering with The University of

Oklahoma, Norman, OK, USA. His current research interests include dynamical system estimation and controls, optimization, machine learning, renewable energy systems, energy storage, and advanced lithium-ion battery management systems.

Dr. Zhang was a recipient of the American Society of Mechanical Engineers (ASME) Energy System Best Paper Award and the Finalist at the 2020 American Control Conference (ACC) and the 2020 Dynamic Systems and Control Conference (DSCC).



Saehong Park received the B.S. and M.S. degrees in electronic engineering from Sogang University, Seoul, South Korea, in 2013 and 2015, respectively, and the Ph.D. degree in civil and environmental engineering from the University of California at Berkeley, Berkeley, CA, USA, in 2020.

He is currently a Post-Doctoral Research Associate with the University of California at Berkeley. His current research interests include optimal and adaptive controls, system identification, energy conversion systems, smart grid systems, and batteries.

Dr. Park has been nominated for the Best Student Paper Award from the American Control Conference in 2018.



Luis D. Couto received the bachelor's degree in chemical engineering from Simón Bolívar University, Caracas, Venezuela, in 2013, the master's degree in renewable energies from the Autonomous University of Madrid, Madrid, Spain, in 2014, and the Ph.D. degree from the Free University of Brussels, Brussels, Belgium, in 2018.

In 2020, he was a Visiting Scholar with the Department of Engineering Science, University of Oxford, Oxford, U.K. He is currently a Post-Doctoral Researcher with the Department of Control Engi-

neering and System Analysis, Free University of Brussels. His current research interests include state/parameter estimation, fault diagnosis, and optimal control in the context of battery management systems.



Venkatasubramanian Viswanathan received the B.S. degree from IIT Madras, Chennai, India, in 2008, and the Ph.D. degree from Stanford University, Stanford, CA, USA, in 2013.

He is currently an Associate Professor with the Department of Mechanical Engineering, Carnegie Mellon University, Pittsburgh, PA, USA. His research focuses on material design for electrochemical energy systems with specific applications, including lithium-ion (Li-ion) and Li-metal batteries, autonomous experimentation, and battery

electrolytes.

Dr. Viswanathan was a recipient of several awards, including the Office of Naval Research Young Investigator Award in 2019, the Sloan Research Fellowship in Chemistry in 2018, the National Science Foundation CAREER Award in 2016, the American Chemical Society PRF Young Investigator Award in 2014, and the Electrochemical Society Daniel Cubicciotti Award in 2010



Scott J. Moura (Member, IEEE) received the B.S. degree from the University of California at Berkeley, Berkeley, CA, USA, in 2006, and the M.S. and Ph.D. degrees from the University of Michigan, Ann Arbor, MI, USA, in 2008 and 2011, respectively, all in mechanical engineering.

From 2011 to 2013, he was a Post-Doctoral Fellow with the Cymer Center for Control Systems and Dynamics, University of California at San Diego, La Jolla, CA, USA. In 2013, he was a Visiting Researcher with the Centre Automatique et Systems,

MINES ParisTech, Paris, France. He is currently an Assistant Professor and the Director of the Energy, Controls, and Applications Laboratory (eCAL) in civil and environmental engineering with the University of California at Berkeley. He is also an Assistant Professor with the Smart Grid and Renewable Energy Laboratory, Tsinghua-Berkeley Shenzhen Institute, Berkeley. His current research interests include control, optimization, and machine learning for batteries, electrified vehicles, and distributed energy resources.

Dr. Moura was a recipient of the National Science Foundation Graduate Research Fellowship, the UC Presidential Postdoctoral Fellowship, the O. Hugo Shuck Best Paper Award, the ACC Best Student Paper Award (as an advisor), the ACC and ASME Dynamic Systems and Control Conference Best Student Paper Finalist (as a student), the Hellman Fellows Fund, the University of Michigan Distinguished ProQuest Dissertation Honorable Mention, the University of Michigan Rackham Merit Fellowship, and the College of Engineering Distinguished Leadership Award.